REPORT DOCUMENTATION PAGE

Form Approved
OMB No. 0704-0188

1. AGENCY USE ONLY (Leave blank)	2. REPORT DATE	3. REPORT TYPE AND DATES COVERED
	May 26, 1995	Technical Report # 9

4. TITLE AND SUBTITLE Electroactive and Photoactive Rod-Coil Copolymers: Design, Synthesis, and Supramolecular Regulation of Photophysical Properties.

5. FUNDING NUMBERS

N00014-94-1-0540

Kenneth J. Wynne
R & T Code: 3132111

6. AUTHOR(S)

J. A. Osaheni and S. A. Jenekhe

7. PERFORMING ORGANIZATION NAME(S) AND ADDRESS(ES)

Department of Chemical Engineering
University of Rochester
206 Gavett Hall
Rochester, NY 14627-0166

8. PERFORMING ORGANIZATION REPORT NUMBER

9

9. SPONSORING/MONITORING AGENCY NAME(S) AND ADDRESS(ES)

Office of Naval Research
800 North Quincy Street
Arlington, VA 22217-5000

10. SPONSORING/MONITORING AGENCY REPORT NUMBER

11. SUPPLEMENTARY NOTES

Accepted for publication in *J. Am. Chem. Soc.*

12a. DISTRIBUTION/AVAILABILITY STATEMENT

Reproduction in whole or in part is permitted for any purpose of the United States government. This document has been approved for public release and sale; its distribution is unlimited.

12b. DISTRIBUTION CODE

13. ABSTRACT *(Maximum 200 words)*

Two series of electroactive and photoactive rod-coil copolymers have been designed, synthesized, and investigated to explore a new structural motif for organizing molecular and macromolecular materials at the supramolecular structure level for enhanced functional and solid state photophysical properties. The rod-coil copolymers consisting of electroactive and photoactive rodlike conjugated segments and inactive coillike segments, exemplified by poly(1,4-phenylene benzobisthiazole-*co*-decamethylene benzobisthiazole) and poly(1,4-phenylenebisvinylene benzobisthiazole-*co*-decamethylene benzobisthiazole), have semi-flexible (semi-rigid) chains whose flexibility (rigidity), folding, intermolecular interactions, and packing, and hence the solid state supramolecular structure and photophysical properties of the materials, are regulated by copolymer composition. The molecular structure, chain sequence lengths, and copolymer composition were determined by NMR (^{1}H, ^{13}C), FTIR, and UV-Visible spectra. The sequence length distribution of the conjugated rodlike segments predicted from the copolymerization statistics was in good agreement with the ^{1}H NMR results. It is shown that nanocomposites are formed at rod molar fractions of less than 0.5 which also marks a dramatic change in the photophysical properties of the copolymers. The photoluminescence quantum yield varied with copolymer composition, reaching over 6- and 7-fold enhancements compared to the "bulk" pure conjugated polymers. The photoluminescence peak of the rod-coil copolymers varied from 486 to 640 nm which represents emission colors that span the visible (blue to red).

14. SUBJECT TERMS

Rod-coil copolymers; electroactive; photoactive; supramolecular structure; polymer nanocomposites; enhanced luminescence.

15. NUMBER OF PAGES 67

16. PRICE CODE

17. SECURITY CLASSIFICATION OF REPORT	18. SECURITY CLASSIFICATION OF THIS PAGE	19. SECURITY CLASSIFICATION OF ABSTRACT	20. LIMITATION OF ABSTRACT
Unclassified	Unclassified	Unclassified	Unlimited

OFFICE OF NAVAL RESEARCH

GRANT N00014-94-1-0540

R & T Code 3132111

Kenneth J. Wynne

Technical Report No. 9

Electroactive and Photoactive Rod-Coil Copolymers: Design, Synthesis, and Supramolecular Regulation of Photophysical Properties

by

John A. Osaheni and Samson A. Jenekhe

Accepted for Publication

in

Journal of the American Chemical Society

University of Rochester
Department of Chemical Engineering
Rochester, NY

May 26, 1995

TECHNICAL REPORT DISTRIBUTION LIST - GENERAL

Office of Naval Research (1)*
Chemistry and Physics Division
Ballston Tower 1, Room 503
300 North Quincy Street
Arlington, Virginia 22217-5660

Defense Technical Information Center (2)
Building 5, Cameron Station
Alexandria, VA 22314

Dr. James S. Murday (1)
Chemistry Division, Code 6100
Naval Research Laboratory
Washington, D.C. 20375-5000

Dr. Kelvin Higa (1)
Chemistry Division, Code 385
Naval Air Weapons Center
Weapons Division
China Lake, CA 93555-6001

Dr. Peter Seligman (1)
Naval Command, Control and
Ocean Surveillance Center
RDT&E Division
San Diego, CA 92152-5000

Dr. Richard W. Drisko (1)
Naval Civil Engineering
Laboratory
Code L52
Port Hueneme, CA 93043

Dr. Harold H. Singerman (1)
Naval Surface Warfare Center
Carderock Division Detachment
Annapolis, MD 21402-1198

Dr. Eugene C. Fischer (1)
Code 2840
Naval Surface Warfare Center
Carderock Division Detachment
Annapolis, MD 21402-1198

* Number of copies to forward

Revised MS # JA950090L

Electroactive and Photoactive Rod-Coil Copolymers: Design, Synthesis, and Supramolecular Regulation of Photophysical Properties

John A. Osaheni† and Samson A. Jenekhe*

Department of Chemical Engineering and Center for Photoinduced Charge Transfer, University of Rochester, Rochester, New York 14627-0166.

ABSTRACT

Two series of electroactive and photoactive rod-coil copolymers have been designed, synthesized, and investigated to explore a new structural motif for organizing molecular and macromolecular materials at the supramolecular structure level for enhanced functional and solid state photophysical properties. The rod-coil copolymers consisting of electroactive and photoactive rodlike conjugated segments and inactive coillike segments, exemplified by poly(1,4-phenylene benzobisthiazole-*co*-decamethylene benzobisthiazole) and poly(1,4-phenylenebisvinylene benzobisthiazole-*co*-decamethylene benzobisthiazole), have semi-flexible (semi-rigid) chains whose flexibility (rigidity), folding, intermolecular interactions, and packing, and hence the solid state supramolecular structure and photophysical properties of the materials, are regulated by copolymer composition. The molecular structure, chain sequence lengths, and copolymer composition were determined by NMR (^{1}H, ^{13}C), FTIR, and UV-Visible spectra. The sequence length distribution of the conjugated rodlike segments predicted from the copolymerization statistics was in good agreement with the ^{1}H NMR results. It is shown that nanocomposites are formed at rod molar fractions of less than 0.5 which also marks a dramatic change in the photophysical properties of the copolymers. The photoluminescence quantum yield varied with copolymer composition, reaching over 6- and 7-fold enhancements compared to the "bulk" pure conjugated polymers. The photoluminescence peak of the rod-coil copolymers varied from 486 to 640 nm which represents emission colors that span the visible (blue to red).

* To whom correspondence should be addressed.

† Current address: General Electric Research and Development, P.O.Box 8, Schenectady, New York 12301.

INTRODUCTION

Molecular and macromolecular materials are of growing interest in a vast array of technological applications ranging from xerography, solar energy conversion, information storage, information processing and display, to sensors.[1-10] One of the often cited advantages for exploring molecular and macromolecular materials in these applications is the power and promise of "molecular engineering" which through synthetic chemistry could be used to prepare and control materials designed to have specified functions and properties. Diverse molecular architectures and synthetic approaches are being explored as a means to "molecular" or "supramolecular" engineering of functional or multifunctional polymeric materials. Examples include: the biosynthesis of new polymers with controlled molecular structure[11]; three-dimensional dendritic polymers (dendrimers) with controlled surface and interfacial properties[12]; two-dimensional polymers that form sheets and exhibit robust quadratic nonlinear optical response[13]; highly branched conjugated polymers that exhibit photorefractivity.[14] Our primary focus here is on electroactive and photoactive macromolecular materials which are highly conjugated and stiff molecules. Much of the synthetic efforts and "molecular engineering" in this area have been directed to control of the *single-chain* structure and properties.[1-10] Recently, however, we showed that supramolecular structure and morphology, i.e. how the chains or chromophores are packed in the solid state, has dramatic effects on the photophysical properties of polymers.[8-10,15] In particular, we have found that intermolecular or interchromophore excited-state processes such as excimer formation have profound effects on the solid state photophysical processes[9], such as luminescence, energy transfer and charge photogeneration, in conjugated macromolecular materials than previously thought. Control of supramolecular structure and morphology is thus of critical importance to achieving efficient photophysical processes in solid state molecular and macromolecular materials.

Rigid rodlike and flexible coillike conformations are the two extreme topologies of linear polymer chains. We propose to explore rod-coil copolymer chain architectures as a

"supramolecular engineering" approach to macromolecular materials in which the solid-state supramolecular structure and morphology (i.e. chain and chromophore packing) and photophysical properties could be controlled by synthesis. The conceptual approach is illustrated in Figure 1. The rod-coil copolymer chain consists of alternating rigid-rod segments **B** and flexible-coil segments **A**. Clearly, such a rod-coil copolymer chain is a semi-flexible (semi-rigid) linear chain whose flexibility (rigidity) is intermediate and variable between those of the rigid-rod polyB and flexible-coil polyA. Our expectation is that by varying the copolymer composition, for a given set of building blocks **A** and **B** and their associated molecular parameters, the rod-coil chain flexibility, intermolecular interactions, folding, and packing in the solid state could be varied from the ordered (nematic liquid crystal-like) or semi-ordered (fringed micelle-like) to the disordered (nanocomposite) supramolecular structures and morphologies shown in Figures 1b, 1c, and 1d, respectively. This kind of variation and control in supramolecular structure and morphology should allow one to control various physical and photophysical properties[9] such as luminescence, photoconductivity, charge transport, energy transfer, and third-order nonlinear optical response.[16] We wish to point out that while our current work on electroactive and photoactive rod-coil copolymers was in progress,[16] the synthesis and nanophase-separation behavior of a rod-coil diblock copolymer consisting of a polyester block and a polyisoprene block were reported.[17] However, the goals, approaches, and rod-coil systems of our work are very different from those of the cited report.[17]

In this paper, we report the synthesis, molecular structure, chain sequence length structure, and investigation of the photophysical properties of two series of rod-coil copolymers, poly(benzobisthiazole-1,4-phenylene-*co*-benzobisthiazole decamethylene) (PBZT-*co*-PBTC10, **4**) and poly(benzobisthiazole-1,4-phenylenebisvinylene-*co*-benzobisthiazole decamethylene) (PBTPV-*co*-PBTC10, **5**), which exemplify a "supramolecular engineering" approach to solid-state electroactive and photophysical properties in macromolecular materials. The molecular structures of these rod-coil copolymers are shown in Chart I along with the structures of the

limiting rigid-rod homopolymers (polyB), poly(1,4-phenylene benzobisthiazole) (PBZT, **1**) and poly(1,4-phenylene bisvinylene benzobisthiazole) (PBTPV, **3**) and flexible-coil homopolymer (polyA) poly(decamethylene benzobisthiazole) (PBTC10, **2**). The molecular structure, copolymer composition, chain sequence lengths, morphology, electroactivity, and photophysical properties of the series of rod-coil copolymers were characterized in detail as reported here. The results show that the photophysical properties (e.g. luminescence quantum yield, emission color) are regulated by the supramolecular structure which in turn is tunable by a synthetic parameter--the rod-coil copolymer composition. The luminescence properties of some members of copolymers **4** have been reported in a short communication.[16a,b] The rod-coil copolymer architecture reported here has also allowed us to demonstrate highly efficient and supramolecular regulation of electronic energy migration and transfer in thin film macromolecular nanostructure assemblies reported elsewhere.[16c]

EXPERIMENTAL SECTION

Materials. 2,5-Diamino-1,4-benzenedithiol dihydrochloride (DABDT) was obtained from Daychem Inc. (Dayton, OH) and was purified by recrystallization as previously reported.[18] Terephthalic acid (>99%, Fluka) and 1,10-decanedicarboxylic acid (99%, Aldrich) were used as received. 1,4-Phenylenediacrylic acid (98%, Aldrich) was recrystallized prior to use, as previously reported.[18b] Polyphosphoric acid (PPA) and 85% phosphoric acid (ACS reagent grade) were purchased from Aldrich Chemical and used to prepare 77% polyphosphoric acid, the polymerization medium. Phosphorous pentoxide (P_2O_5) was obtained from Baker Inc and used as received.

Synthesis. The synthesis and characterization of the conjugated rigid-rod homopolymers[18a,b] **1** and **3** and the coillike homopolymer **2**[18c] have been reported.[18]

Copolymers 4, PBZT-*co*-PBTC10. The following procedure exemplifies the synthesis of the 8 different compositions of the rod-coil copolymers **4a-4h**.

In the synthesis of **4c**, a total of 0.8 g (3.26 mmol.) of DABDT was dissolved in 11 g of 77% PPA (dearated) in a glass reactor vessel fitted with a mechanical stirrer, two gas ports, and a side arm. The reaction vessel was purged with nitrogen for 30 min and dehydrochlorination (i.e. removal of 2HCl from DABDT) was carried out at 70 °C under vacuum. After complete dehydrochlorination, the reaction vessel was cooled down to 50 °C, and 0.11 g (0.65 mmol., i.e. 20 mole%) of terephthalic acid and 0.6 g (2.61 mmol., i.e. 80 mole%) of 1,10-decanedicarboxylic acid were added under positive N_2 pressure. The reaction mixture was stirred for 30 min to ensure intimate mixing of the monomers, and 5 g of fresh P_2O_5 was added to compensate for the calculated theoretical water of condensation. The temperature was progressively raised to 100 °C for 4 h, then to 140 °C for 6 h and finally to 180 °C and held at this temperature for 10-16 h for the different compositions. The highly viscous polymerization dope (yellow in color) was precipitated in a large volume of water. The fibrous product was washed several times with water and shredded into small pieces with a blender. The copolymer was subsequently purified by refluxing in water for 2 days. The yield was 100%. Intrinsic viscosity [η] = 5.3 dL/g (30 °C in methanesulfonic acid); ^{1}H NMR ($CD_3NO_2/AlCl_3$, ppm) : δ = 1.2-1.7 (m, 12H), 2.0 (t, 4H), 3.6 (t, 4H), 8.6 (d, 4H), 9.0 (s, 2H), 9.2 (d, 2H), 9.3 (s, 2H). FTIR (free standing film, cm^{-1}) 3055, 2923, 2851, 1603, 1533, 1484, 1465, 1428, 1405, 1311, 1273, 1247, 1210,1158, 1113, 1085, 1056, 1005, 960, 860, 843, 722, 688, 629, 611. ^{13}C NMR ($CD_3NO_2/AlCl_3$, ppm): δ = 28.4-28.83, 29.01-29.04, 32.11-32.23, 113.41, 130.95-131.16, 131.78, 132.78, 138.17, 188.3, 188.42-188.85.

The synthesis of the other 7 copolymers **4** was similar. The main difference was in the ratio of the terephthalic acid to the 1,10-decanedicarboxylic acid. The reaction yields were typically 99-100%. The ^{1}H NMR resonances and the FTIR bands of the other copolymers **4a**, **4b**, **4d**, **4e**, **4f**, **4g**, and **4h** were identical to those of **4c**, within ±2 cm^{-1}, in the case of the FTIR spectra.

Copolymers 5, PBTPV-*co*-PBTC10. The following procedure is typical for the synthesis of the different compositions of the rod-coil copolymers **5a-5h**.

In the synthesis of **5c**, a total of 0.8 g (3.26 mmol.) of DABDT was dissolved in 14 g of 77% PPA (dearated) in the glass reactor vessel described above. The reaction vessel was purged with nitrogen for 30 min and dehydrochlorination was carried out at 70 °C under vacuum. After complete dehydrochlorination, the reaction vessel was cooled down to 50 °C, and 0.142 g (0.65 mmol., i.e. 20 mole%) of 1,4-phenylene diacrylic acid and 0.6 g (2.61 mmol., i.e. 80 mole%) of 1,10-decanedicarboxylic acid were added under positive N_2 pressure. The reaction mixture was stirred for 30 min to ensure intimate mixing of the monomers, and 6 g of fresh P_2O_5 was added to compensate for the calculated theoretical water of condensation. The temperature was progressively raised to 100 °C for 4 h, then to 140 °C for 2 h and finally to 160 °C and held at this temperature for 12-14 h for the different compositions. The highly viscous polymerization dope (orange in color) was precipitated in a large volume of water. The fibrous product was washed several times with water and shredded into small pieces with a blender. The copolymer was subsequently purified by refluxing in water for 2 days. The yield was ~99%. $[\eta]$ = 5.0 dL/g (30 °C in methanesulfonic acid); ^{1}H NMR ($CD_3NO_2/AlCl_3$, ppm) : δ = 1.2-1.7 (m, 12H), 2.1 (t, 4H), 3.7 (t, 4H), 7.9 (d, 2H), 8.1 (m, 4H), 8.4 (d, 2H), 8.9 (m, 6H). FTIR (free standing film, cm^{-1}) 3033, 3000, 2923, 2852, 1696, 1624, 1528, 1490, 1464, 1426, 1404, 1310, 1261, 1233, 1180, 1162, 1108, 1055, 950, 858, 805, 722, 689, 660, 636. The ^{1}H NMR resonances and the FTIR absorption bands of the other copolymers **5a**, **5b**, **5d**, **5e**, **5f**, **5g**, and **5h** were identical to those of **5c**, within ± 2 cm^{-1} in the case of the FTIR spectra.

Characterization. The intrinsic viscosity $[\eta]$ of the polymers and copolymers was measured in methanesulfonic acid at 30 °C by using a Cannon Ubbelohde capillary viscometer. Thermogravimetric analysis (TGA) and differential scanning calorimetry (DSC) were done by using a Du Pont Model 2100 Thermal Analyst based on an IBM PS/2 Model 60 computer and equipped with a Model 951 TGA and a Model 910 DSC units. The TGA data were obtained in flowing nitrogen at a heating rate of 10 °C/min whereas the DSC thermograms were obtained in nitrogen at a heating rate of 20 °C/min. FTIR spectra were taken on free standing films of the polymers at room temperature using a Nicolet Model 20SXC Fourier transform infrared (FTIR)

spectrometer under nitrogen purge. The ^{1}H NMR and ^{13}C NMR spectra were taken at 300 MHz by using a General Electric Model QE 300 instrument. Polymer solutions for ^{1}H NMR and ^{13}C NMR spectra were prepared in a dry box, using deuterated nitromethane containing aluminum trichloride as the solvent. Solution processing of the polymers into films was achieved by using the method of reversible coordination complexation approach.[19] Thin films of good optical quality were prepared by spin coating of nitromethane/$AlCl_3$ solution of the copolymers onto glass substrates, followed by decomplexation in deionized water to obtain films of the pristine copolymers.

The morphology of the polymers were observed with an Olympus Model BH-2 microscope in conjunction with a Mettler Model FP82 hot stage and Model FP90 Central Processing Unit (controller). X-ray powder diffraction of free standing films of the homopolymer PBTC10 (**2**) and PBZT-*co*-PBTC10 copolymers **4b**, **4c**, **4d**, and **4g**, was obtained at Oneida Research (Whitesboro, NY) on a Siemen D500 automated powder diffractometer equipped with a graphite monochromator. The instrument was set up with a Cu radiation (λ = 1.54 Å) X-ray source operating at 50 kV and 40 mA. The two-theta scan range was set to be 4-80° using a step scan window of 0.05°/1.0 second step. Beam slits were set at 1°, 1°, 1°, 0.15°, and 0.15° widths. Two-theta calibration was performed using an National Bureau of Standards (NBS) mica standard (SRM 675). Data were collected and reduced with the use of a Micro VAX II computer.

Optical absorption spectra of thin films and solutions of the copolymers and homopolymers were obtained with a Perkin Elmer Model Lamda 9 UV-Vis-near IR spectrophotometer in the wavelength range 190-3200 nm. Steady state photoluminescence studies were done by using a Spex Fluorolog-2 Spectrofluorometer equipped with Spex DM3000f Spectroscopy computer. Fluorescence measurements were made on 20-100 nm thin films. The polymer or copolymer thin films were positioned such that the emission was detected at 22.5° from the incident radiation beam. Fluorescence quantum efficiencies were obtained by comparing the integration of the emission spectra (in wavenumbers) of the samples (unknown) with that of a known standard in the same optical configuration using the relation[20]:

$$\Phi_u=[(A_sF_un^2)/(A_uF_sn_0^2)]\Phi_s \quad (1)$$

where subscripts u and s refer to the unknown and the standard, respectively, A is the absorbance at the excitation wavelength, F is the integrated emission area across the band, n is the refractive index of the unknown sample, and n_0 is the refractive index of the standard. The refractive indices were assumed to be close and hence no correction was made. Variation in the intensity of the exciting source with wavelength was accounted for by taking the spectra in the ratio mode (s/r); that is, by dividing the signal with that of rhodamine B which is used as the internal standard. We used a thin film of ~10^{-3}M 9,10-diphenylanthracene in poly(methylmethacrylate) (PMMA) as a standard (Φ_f = 83%)[21a] for the thin films and quinine sulfate (~10^{-6}M in 0.1N H_2SO_4) (Φ_f = 55%) as the fluorophore standard[21b] for the solutions. Time-resolved photoluminescence decay measurements were performed by using the time-correlated single photon counting (SPC) technique. The excitation system consisted of a cavity dumped dye laser (Coherent Model 703D) circulating rhodamine 6G, synchronously pumped by a mode-locked frequency doubled Nd:YAG laser (Quantronics Model 416). The dye laser pulses were typically of 10 ps duration at a repetition rate of 38 MHz. The samples were excited at 380 nm. All the photophysical measurements were done at room temperature.

Cyclic voltamograms of thin films of some of the copolymers were obtained by using an EG&G Princeton Applied Research Potentiostat/Galvanostat Model 270 equipped with Electrochemical Analysis System software based on IBM PS/2 Model 60 computer. Platinum wires were used as both the counter and working electrodes and Ag/Ag^+ (silver wire in 0.1M $AgNO_3$ in electrolyte solution) was used as a reference electrode. The Ag/Ag^+ was calibrated with ferrocene as the internal standard. Thin films of copolymers **4** or **5** on platinum electrodes were prepared by dipping the electrode into a 0.5-1.0 wt% copolymer solution in nitromethane-$AlCl_3$ and the resulting film rigorously washed and dried in the vacuum oven at 80 °C, as described above. A 0.1M tetrabutylammonium tetrafluoroborate (TBABF4) (Aldrich) in ultra pure acetonitrile (99+%, Johnson Matthey Electronics) was used as the electrolyte. The potential

values were referenced back to the SCE potential by using the ferrocene/ferrocenium couple as an internal standard. The scan rate was 20 mV/s.

RESULTS AND DISCUSSION

Synthesis, Molecular Structure, and Composition

The rod-coil copolymers **4** and **5** were synthesized by condensation copolymerization of the tetrafunctional monomer 2,5-diamino-1,4-benzenedithiol (DABDT) with aromatic and aliphatic diacids as illustrated in Scheme I. This relatively simple reaction scheme is quite versatile in its ability to generate diverse macromolecular materials with the rod-coil linear chain architecture of Figure 1. Among the synthetic parameters that can be readily manipulated include the rod fraction $f = x/(x+y)$, the aspect ratio which is determined by the Ar moiety and the rod block chain length x, and the flexibility of the rod-coil chain which is determined by the number of methylene groups z and the coil block chain length y. For the present series of copolymers **4** and **5**, the number of flexible methylene groups was fixed at 10. Eight members of each series of rod-coil copolymers (**4a-4h** and **5a-5h**, Chart I), representing compositions f of 5 to 80 mol% rods were prepared with quantitative reaction yields (99-100%).

The molecular structures and compositions of the rod-coil copolymers were established primarily by ^{1}H NMR, ^{13}C NMR and FTIR spectra which are submitted as Supplementary Material. The solution ^{1}H NMR and ^{13}C NMR spectra were obtained in nitromethane-$AlCl_3$ in which the Lewis acid helps to solubilize all the copolymers and homopolymers, facilitating the solution spectroscopic characterization of the materials as we have previously demonstrated in other heterocyclic rigid-chain polymers.[19] The ^{1}H NMR spectra of all the copolymers **4** and **5** were found to be in excellent agreement with the proposed structures. The copolymer compositions in the form of the molar ratio $f = x/(x+y)$ were readily determined from the ratio of the 1,4-phenylene ring or *trans*-vinylene proton resonance to the aliphatic methylene proton resonances and were in excellent agreement with the feed compositions as shown in Figure 2. This is consistent with the quantitative yields (99-100%) achieved in the polymerizations and the statistically random nature of the rod-coil copolymers.

The FTIR spectra were in excellent agreement with the proposed structures, giving the expected characteristic vibrational bands [22-25] and changes with copolymer composition *f*. Linear relationships between *f* determined from FTIR spectra and feed compositions of **4** and **5** were obtained, providing an independent check of the NMR data.

Table 1 shows some of the physical properties of copolymers **4** and **5**. The intrinsic viscosity [η] values, measured in methanesulfonic acid at 30 °C, are between 3.5-7.0 dL/g, indicating that these semi-flexible (semi-rigid) rod-coil copolymers have high molecular weights. The intrinsic viscosities of the homopolymers **1-3** (PBZT, PBTC10, and PBTPV) are also tabulated for comparison. The intrinsic viscosity of the copolymers lies between the two extremes of the flexible coil [η]=3.3 dL/g and the rigid-rod polymers ([η]=32 dL/g for **1** and [η]=5 dL/g for **3**). The much lower intrinsic viscosity values of copolymers **4** compared to the rigid-rod polymer **1** (PBZT) suggests that the average sequence lengths of rodlike segments consisting of PBZT repeat units are not very long and that the chain rigidity of the copolymers is very different from the homopolymer. Using the known Mark-Houwink[26] relation for PBZT (**1**), the molecular weight of a PBZT with intrinsic viscosity of 32 dL/g is 40,200, corresponding to a chain length of 151 repeat units. The TGA thermograms of all the homopolymers and copolymers were obtained in flowing nitrogen atmosphere at a heating rate of 10 °C/min. A summary of the onset of thermal decomposition of all copolymers **4** and **5** is given in Table 1. The thermal stability of the copolymers is only slightly enhanced compared to the flexible-coil polymer **2**, and is much lower than that of the π-conjugated homopolymers **1** and **3**. From Table 1, it is seen that the thermal stability of copolymers **4** and **5** are quite similar, with onset of decomposition at ~450-470 °C. The thermal stability of the copolymers is thus largely limited by the methylene groups in the backbone.

Chain Sequence Length Distribution

The segmented rod-coil chain architecture of Figure 1a and copolymers **4** and **5** (Chart I) in which rodlike segments alternate with coillike segments can be denoted compactly as $\mathbf{B}_x\mathbf{A}_y$, where the segment chain lengths x and y are statistical in nature. In addition to the overall

composition f (= x/(x+y) the distribution of the segment chain lengths x and y are critical to the conformations, flexibility, chain packing, and physical properties of the rod-coil copolymers. These segment length distributions are determined by the nature of the polymerization process.[25,27-28] Our step copolymerizations of Scheme I are expected to result in *random segmented copolymers* irrespective of the differences in the reactivities of the monomers.[27] Thus, expressions for the sequence length distribution can be derived from probability considerations described in detail in the Supplementary Material. Let p be the probability that a condensation reaction occurs between 2,5-diamino-1,4-benzenedithiol (DABDT) and a *rod-forming* monomer **B** (e.g. terephthalic acid), (1-p) is the probability that a condensation reaction occurs with a *coil-forming* monomer **A** (i.e. 1,10-decanedicarboxylic acid). The probability P(x) that the rodlike sequence $\mathbf{B}_x$ has been formed is

$$P(x) = (x+1)p^x(1-p)^2 \qquad ; 0 < p < 1 \; ; \sum_{x_1}^{\infty} P(x) = 1 \qquad (2)$$

P(0), is the probability that both ends of DABDT react with coil-forming **A** and is numerically identical to $(1\text{-p})^2$. Since condensation polymerization is independent of monomer reactivity[27], the probability p is identical to the monomer feed ratio which is the molar ratio of **B** to **A**.

Figure 3 shows the probability distribution of block sizes of rigid-rod segments $\mathbf{B}_x$ in chains of rod-coil copolymer **4e** which contains 40 mol% rods (PBZT repeat units). The block size 0 represent the flexible-coil segments $\mathbf{A}_y$. Rigid-rod segments $\mathbf{B}_x$ with block sizes of 1, 2, 3, 4, 5, and 6 are clearly evident in Figure 3. The associated physical lengths of the calculated $\mathbf{B}_x$ distributions in terms of PBZT (**1**) repeat units incorporated into each rodlike segment in the copolymer **4** chains can be estimated from the X-ray diffraction data for the monomeric model compound and our recent computational modeling of PBZT and its oligomers.[15] The PBZT repeat unit has a length of 1.25 nm, a thickness of ~0.35 nm and a width of 0.6 nm. Thus, the approximate block lengths l_x of rodlike segments $\mathbf{B}_x$ in **4e** are: l_1 = 2.1 nm; l_2 = 3.3 nm; l_3 = 4.6 nm; l_4 = 5.8 nm; l_5 = 7.1; and l_6 = 8.3 nm. Figure 3 also shows that the most probable rodlike segment is $\mathbf{B}_1$ which has a block of length 2.1 nm. Similar computation of the probability distributions of $\mathbf{B}_x$ in other copolymers **4a**, **4b**, **4c**, and **4d**, revealed that the most probable

rodlike segment chain length is x=1. The distributions of the π-conjugated rodlike blocks $\mathbf{B}_x$ in rod-coil copolymers **5** are expected to be identical to those of copolymers **4** since both were synthesized by the same condensation reaction Scheme I and reaction conditions.[27] In the case of copolymers **5**, we estimate the physical length of $\mathbf{B}_1$ to be approximately l_1 =2.7 nm which indicates that the rodlike segments $\mathbf{B}_x$ in **5** are longer than the corresponding **4**. The other block lengths l_x of the rodlike segments $\mathbf{B}_x$ in **5a**-**5e** are expected to be l_2 = 4.4 nm; l_3 = 6.3 nm; l_4 = 8.1 nm; l_5 = 9.9 nm; l_6 = 11.7 nm and l_7 = 13.5 nm.

Information on the chain sequence length distributions is also contained in the ^{1}H NMR spectra of the copolymers[28,29], since the chemical shifts of the protons on the benzobisthiazole rings are sensitive to the structural environments. The total fraction of the -AA- sequence which refers to the total distribution of two or more adjacent coillike sequence $\mathbf{A}_y$, can be determined from the integration of the resonance at 8.9 ppm, compared with the integration of the -AB- and -BB- resonances at 9.2 and 9.3 ppm, respectively. The proton resonances of -AB- or -BA- arise from benzobisthiazole rings linked to *both* rod-forming 1,4-phenylene and coil-forming -$(CH_2)_{10}$- moieties. Similarly, -BB- proton resonances at 9.3 ppm is a result of benzobisthiazole rings linked to *only* 1,4-phenylene rings on either side. A plot of the probability distribution, P(0), of -AA- sequence and the ^{1}H NMR integration as functions of feed composition are shown in Figure 4. There is a remarkable agreement between the predicted distribution and the experimentally measured -AA- sequence. Also, the statistical model predicts a sequence of predominantly -AA- and -AB- in **4a** and **4b**, hence **5a** and **5b**, in agreement with the ^{1}H NMR results which show essentially two resonances for the benzobisthiazole protons at 8.9 and 9.2 ppm in these "dilute" rod compositions. Thus, the distribution of the other block sizes using this probability model as shown in Figure 5 should be reasonably close to the actual sequence distribution in these copolymers.

Phase Behavior and Morphology

The phase behavior and morphology of the copolymers were investigated by differential scanning calorimetry (DSC), polarized optical microscopy and wide angle X-ray diffraction

(WAXD) (submitted as Supplementary Material). The melting temperature observed in the homopolymer PBTC10 (232 °C) was progressively elevated in **4a** and **4b** to 247 and 262 °C, respectively, and the corresponding enthalpy of fusion progressively decreased. Similar observations on the melting transition were seen in **5a** and **5b**. The DSC thermograms of copolymer compositions greater than 10% did not show either a glass transition or melting in repeated scans up to 350 °C, similar to the pure PBZT. The results indicated that phase separation of the rods and coils[30] does not occur with heating of the copolymers containing greater than 10% rods. The results also suggest that the thermophysical properties of the copolymers, even at 20% rods, are already significantly enhanced relative to the coil homopolymer **2**. Observation of the copolymers films of greater than 10% rods with optical microscopy under crossed polarizers revealed that the films were isotropic, even when heated on a hot stage to 300 °C. The disordered and amorphous morphology of the copolymers was also confirmed by wide angle X-ray diffraction (WAXD). The disordered nature of these copolymers, at $f < 0.5$, arises from the random distribution of rods of different lengths in the matrix of the flexible coil as in Figure 1d.

A model of the assembly of the rod-coil copolymer chains at one copolymer composition f is shown in Figure 6. This model of the supramolecular structure and morphology of the segmented rod-coil copolymers which takes into account all the characterizations, including the chain sequence distributions, is very similar to the disordered (nanocomposite) morphology of Figure 1d.

Photophysical Properties

Absorption Spectra. UV-visible absorption spectroscopy of thin films of the rod-coil copolymers **4** and **5** was done to gain insight into the evolution of the electronic structure with composition. Figure 7 shows the optical absorption spectra of selected copolymers **4** (**4a**, **4c**, **4e**, **4f**, **4h**) along with the spectrum of the conjugated homopolymer **1** (PBZT). The coillike nonconjugated polymer **2** (PBTC10), and consequently coillike segments $\mathbf{A}_y$ of the segmented copolymer $\mathbf{B}_x\mathbf{A}_y$, does not absorb in the 340-600 nm spectral range. This means that the

copolymer absorption spectra seen in Figure 7 largely reflect the conjugated rodlike segments $\mathbf{B}_x$ in the copolymers. Starting with copolymer **4a** absorption (curve 6 in Figure 7), one sees a highly structured spectrum with five overlapped peaks in the 345-440 nm region and an overall absorption maximum (λ_{max}) centered at 385 nm. These basic features of copolymer **4a** absorption were also observed in the absorption spectra of copolymers **4b**-**4e**. At higher rod compositions, as in copolymers **4f**-**4h**, the peaks in the absorption spectra are largely merged and the overall spectra are progressively red-shifted as the composition dependence of the copolymer absorption maximum (λ_{max}) shows in Figure 8. A significant feature of the copolymer absorption spectra (Figure 7) is the progressive increase of the relative intensity of the peaks at 408, 438, and ~468 nm as the copolymer structure evolved toward the π-conjugated homopolymer **1**. In fact, the absorption spectrum of the homopolymer **1** (Figure 7, curve 1) has vibronic peaks at 408, 438, and 468 nm; these features were already observable in copolymers **4e** which contains 40 mol% **1**.

The absorption spectra of copolymers **5a**-**5e** and **5h**, and of the corresponding homopolymer **3** (PBTPV) are shown in Figure 9. The highly structured absorption spectra observed in copolymers **4** of Figure 7 are also seen in copolymers **5** of Figure 9. The main difference between the absorption spectra of the two series of rod-coil copolymers is that copolymers **5** have absorptions that are red-shifted from those of the repeat unit of **3** incorporated in the rodlike segments of **5**. The absorption maximum (λ_{max}) in the copolymer spectra of **5a**-**5e** is identical at 425 nm but it progressively increases with composition in **5f**-**5h** as shown in Figure 10. The vibronic peaks at 508 and 475 nm and shoulder at 450 nm observed in the absorption spectrum of the conjugated homopolymer **3** are already observable in the absorption of copolymer **5c**, i.e. at 20 mol% rods.

Although the conjugation length distribution of the copolymers in terms of the rodlike conjugated oligomers $\mathbf{B}_x$ incorporated into the rod-coil copolymers $\mathbf{B}_x\mathbf{A}_y$ was determined from NMR spectra and copolymerization statistics, the vibronic peaks in the UV-visible spectra of the copolymers could not be quantitatively assigned or deconvoluted. This is because of the overlaps

of the different oligomer $\mathbf{B}_x$ (x=1, 2, 3, ...) absorption spectra at each copolymer composition as well as the absence of known absorption spectra for individual oligomers within the distribution in a copolymer. Only the monomeric model compound of **4**, 2,6-diphenylbenzo[1,2-d:4,5-d']bisthiazole, has a known absorption spectrum which has vibronic peaks at 333, 347, and 364 nm and maximum absorption at 347 nm. Absorption features close to these are convoluted in the copolymer absorption spectra of **4**. Thus, deconvolution techniques such as those successfully applied to the absorption spectra of triblock copolymers containing polyenes of 4-16 conjugated double bonds[32] could not be used here to analyze the spectra of copolymers **4** and **5**. Nevertheless, important conclusions can be drawn from the absorption spectra of the copolymers **4** and **5**.

The observed similarity of the absorption maximum (λ_{max}) in the spectra of copolymers **4a-4e** is in accord with the most probable sequence distribution predicted from the copolymerization model to be the same in the 5-40 mol% composition region. The copolymer absorption spectra (Figures 7-10) also graphically illustrate the step-by-step nature and the statistics of condensation copolymerization.[27]

The optical absorption bands in the copolymer absorption spectra arise from the highest occupied molecular orbital (HOMO)-Lowest unoccupied molecular orbital (LUMO) or π-π^* transitions of the discrete chromophores $\mathbf{B}_x$, incorporated into the rod-coil copolymers. The presence of the same vibronic peaks observed in the π-conjugated homopolymers at the same energies in the copolymers with conjugated segments of only 20-40 mol%, where short discrete-sized chromophores ($\mathbf{B}_x$, $x<<10$) exists, confirms the validity of the notion of a "distribution of conjugation length" model[33] of π-conjugated polymers and suggests a molecular (exciton) origin of the photoexcitation in the conjugated homopolymers **1** and **3**. We estimate that the average conjugation lengths in the conjugated polymers **1** (PBZT) and **3** (PBTPV) to be no more than 5-6 repeat units or in terms of physical lengths of the rodlike molecules 7-8 nm in **1** and 10-12 nm in **3**.

Important effects of *chromophore size* and *spatial confinement* of chromophores on the electronic structure are observed when the composition dependent copolymer absorption spectra are compared to those of the pure conjugated homopolymers. As the physical length of the chromophore is reduced below that of the conjugated homopolymer, i.e. $f < 1$, both the absorption λ_{max} and absorption edge progressively shift to higher energy. However, the clearly well resolved vibronic structure in the copolymer absorption spectra (Figures 7 and 9) appear only at compositions below 50 mol% ($f < 0.5$) where there is both reduced chromophore size and three-dimensional spatial confinement as the rodlike chromophores are dispersed in the coillike matrix (Figure 1d). This implies that the rod-coil copolymers in this composition region are "quantum boxes" or nanocomposites in which excitons could be confined. In the light of such possibility, the entire rod-coil copolymers represent excellent model systems for testing theoretical ideas about the effects of spatial confinement, size restriction, chain topology, intermolecular interactions, π-conjugation length distribution, and supramolecular structure on the electronic, photophysical, and nonlinear optical properties of macromolecular materials.[7,9,33-35]

Luminescence Spectra.

Effects of the rod-coil copolymer composition *f* and supramolecular structure on the solid state luminescence was investigated by measuring the steady state photoluminescence (PL) spectra, PL quantum yield Φ_f, and time-resolved PL decay dynamics as a function of composition *f*. Figure 11 shows the steady state PL spectra of thin films of several copolymers (**4a, 4c, 4e, 4h**) and the corresponding homopolymer **1** (curve 1), indicating that the emission color can be tuned between the extremes of yellow (**1**) and blue (**4a**). Similar PL spectra of thin films of copolymers **5a, 5b, 5c**, and **5f** along with the spectrum of the homopolymer **3** are shown in Figure 12. By virtue of the smaller HOMO-LUMO or π-π^* excitation energies of the chromophores of **5** and **3**, compared to **4** and **1** respectively, a wider range of tunability of the emission color between the extremes of red (**3**) and blue (**5a**) is obtained. The variation of the emission λ_{max} with composition *f* of the two series of copolymers **4** and **5** are shown in Figures 8

and 10, respectively, revealing a large apparent Stokes shift between the emission and absorption λ_{max}. A number of interrelated issues regarding the features of these emission spectra and their composition dependence warrant a detailed discussion, including: the nature of the emitting species; the wide variation of the emission λ_{max} with composition; and the origin of the large apparent Stokes shift.

In copolymers **4**, the emission spectrum of **4a** (curve 5, Figure 11) has vibronic structure and is nearly a mirror image of the absorption spectrum. The structure in the emission spectrum of **4a** appears to be a result of the overlap of four or more emission bands. In contrast, the emission spectra of all the remaining copolymers **4** ($f > 10\%$) have broad and structureless lineshape similar to the emission of the conjugated polymer **1**. The emission spectra of **5a** and **5b** have vibronic structure whereas broad and structureless emission lineshapes are observed in the copolymers **5c-5h** and **3** (Figure 12). We recently established that the broad and structureless thin film emission spectra of conjugated polymers **1** and **3** originated from excimer emission as a result of chromophore aggregation.[9] The "single chromophore" or "monomer" emission of these and other conjugated polymers was observed in dilute (~0.05 wt%) blends with nonconjugated flexible-chain polymers.[9] Thus, excimer emission can be expected in these rod-coil copolymers depending on the rod composition f which determines both the interchromophore distances and their overall spatial distribution. In the $f \geq 50\%$ copolymers where the coillike segments are dispersed in the rodlike segments, as illustrated in Figure 1c, the similarity of chromophore aggregation to the "bulk" conjugated polymers suggests excimer emission. Even in the $f < 50\%$ copolymers, except for the possible exception of **4a** and **5a-5b**, *inter*chain and *intra*chain excimer formation cannot be completely eliminated. An alternative, and perhaps complementary, interpretation of the broad and structureless emission spectra in the $f < 50\%$ copolymers is inhomogeneous broadening resulting from the distribution of the HOMO-LUMO excitation energies and the corresponding distribution in the energy levels of the emitting states of chromophores $\mathbf{B}_x$.

It has been suggested that the large apparent Stokes shift between the emission and absorption maxima ($\Delta\lambda_{max}$) in π-conjugated polymers (~0.3-0.7 eV) is a result of excitation migration and transfer to the lowest π-π^* excitation energy chromophore from which emission occurs.[33] However, the discovery of excimer emission in conjugated polymers and the finding that the "single chromophore" emission of these materials has little or no Stokes shift now provide the correct interpretation of $\Delta\lambda_{max}$ in terms of the stabilization energy of the excimers.[9] Excimer emission also accounts for the large $\Delta\lambda_{max}$ in the $f \geq 50\%$ copolymers (Figures 8 and 10). Copolymers **4a**-**4e** and **5a**-**5e** which contain discrete-sized chromophores of known size and HOMO-LUMO gap distributions provide an additional test of and evidence against the idea of emission from the lowest π-π^* energy chromophore in an essemble of spatially distributed chromophores of different π-π^* excitation energies. The chromophore distribution and π-π^* excitation energy distribution in each of the copolymers **4a**-**4e** (or **5a**-**5e**) are the same and yet there is a wide variation of emission λ_{max} with composition (Figures 7-10). Furthermore, the excitation wavelength (λ_{ex}) was identical in the PL spectra of **4a**-**4e** (λ_{ex} = 384 nm) and in the PL spectra of **5a**-**5e** (λ_{ex} = 425 nm). Emission from the smallest energy chromophore would have resulted in identical emission peak in each copolymer series in the $f < 50\%$ range, contrary to what was actually observed. The most plausible reason for the emission λ_{max} variation in the $f < 50\%$ copolymers is the variation in spatial confinement and spatial distribution (i.e. variation in supramolecular structure) of chromophores in addition to the distribution in the HOMO-LUMO excitation energies.

Figure 13 shows the composition dependence of the PL quantum yield $\Phi_f(f)$ in the two series of copolymers **4** and **5**. The homopolymers **1**, **2**, and **3** have Φ_f values of ~6, 7×10^{-2}, and 4%, respectively. Two regions of composition ($f \geq 50\%$ and $f < 50\%$) are defined by the quantum yield data of Figure 13. In each of the copolymers with $f \geq 50\%$, the fluorescence quantum yield is virtually the same as the corresponding π-conjugated polymer. A large enhancement of the PL quantum yield is observed in the copolymers when $f < 50\%$. The solid state PL is highest in **4c** with Φ_f ~38% which corresponds to over a 6-fold enhancement compared to the conjugated

polymer **1**. In the copolymers **5**, the largest PL quantum yield is observed in **5a** with Φ_f =29% which is a factor of 7.25 larger than that of the conjugated polymer **3**.

The composition dependent PL quantum yield results can be understood in terms of the variation in the solid state supramolecular structure (chromophore packing and spatial distribution) of the rod-coil copolymers. In the composition region 50 $\leq f$ <100%, the rodlike chromophores are aggregated much like in the bulk π-conjugated polymers, resulting in excimer formation and self-quenching.[9] On the other hand, the spatial confinement and distribution of chromophores in the 0<f<50% copolymers (see Figure 1d) or nanocomposites leads to the observed enhancement of quantum yield as a result of the reduced excimer formation and self-quenching. We point out that, consistent with this interpretation, is the decrease of quantum yield in **4a**-**4b**, compared to **4c**, which is a result of the increased chain flexibility that favors phase separation of the rods and coils[30] as evidenced by the previously discussed differential scanning calorimetry results. Similar decrease of quantum yield at f < 20% in copolymers **5** was not observed because of the higher aspect ratio of the rodlike segments in **5** and consequent greater stiffness of the rod-coil chains compared to **4** at similar compositions. These results demonstrate the supramolecular regulation of solid state PL quantum yield of macromolecular materials through the synthetic parameter f.

The time-resolved (ps) photoluminescence decay dynamics of thin films of several copolymers **4** and the conjugated polymer **1** were investigated. Representative copolymer PL decay dynamics are shown in Figure 14 for **4b**-**4d** and **4h**. The decay dynamics was found to be independent of the intensity of the exciting laser, suggesting that the decay does not proceed by a bimolecular mechanism. The PL decay dynamics of the copolymers progressively improved from a nonexponential decay mechanism in **4h**, to a largely single exponential decay in **4c**, consistent with the observed dependence of the PL quantum efficiency on composition. Analysis of the decay profile shows that the luminescent lifetime of **4c** is 0.9 ns and follows a single exponential profile with an amplitude of ~80%. The other copolymers in the f < 50% composition range could be described with a single exponential radiative decay kinetics to

varying amplitudes of 60-70% and lifetimes in the 0.6-0.7 ns range, as shown in Table 2. The PL decay dynamics of **1** was nonexponential and similar to **4h** and copolymers with $f > 50\%$. These results are consistent with the measured PL quantum efficiencies and the previously discussed effects of copolymer composition and chromophore aggregation on the steady state photoluminescence in general.

All the present results on the solid state luminescence of the rod-coil copolymers can be understood qualitatively by the modified Birks[36-38] photophysical kinetic scheme for excimer forming systems shown in Scheme II:

Scheme II

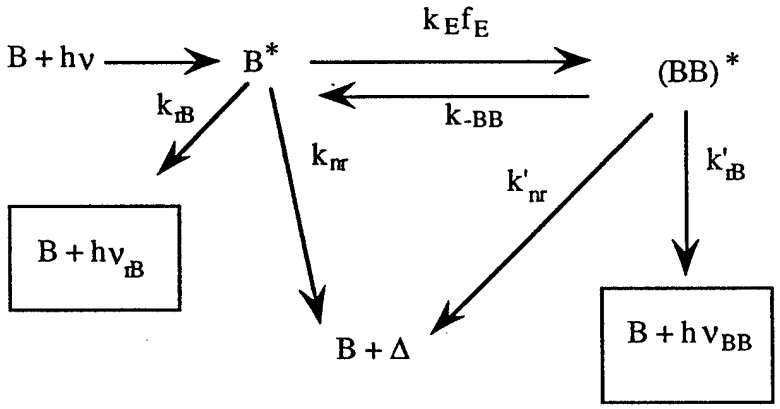

In Scheme II, B is a rodlike chromophore in the sense of Figure 1, B* represents an excited chromophore, (BB)* is an *inter-* or *intra*chain excimer. The rate constants k_{rB} and k'_{rB} are those for the emission from a "single chromophore" and excimer respectively, whereas k_{nr} and k'_{nr} are the corresponding sum of all nonradiative rate constants for deactivation of the excited state species. The parameter k_E represents the rate of energy transfer and f_E is the fraction of preformed excimer sites. Since these rod-coil copolymers did not show any glass transition, only the fraction of aggregated rigid-rod chromophores will contribute to excimer formation. In the pure π-conjugated polymers which have relatively planar geometries and sandwich-type cofacial packing distances of order 3-4 Å,[9,15] the fraction of excimer forming sites is close to unity, hence excimer formation is highly favored and is only limited by the rate constant for energy

transfer (~a few ps). Thus, the observed multiexponential nature of the decay profile of π-conjugated polymers, can be accounted for by this mechanism. The unimolecular nature of excited state decay with corresponding first-order rate constants, allows one to relate the PL quantum yield to the first-order rate constants or excited state lifetimes:

$$\Phi_f = \frac{k_r}{\sum_j k_j} \qquad (3)$$

Scheme II and equation (3) suggest how the control of the supramolecular structure (chromophore aggregation and their spatial distribution) regulates the photophysics of the rod-coil copolymers. Reduction or prevention of chromophore aggregation controls f_E, the spatial distribution of chromophores also controls k_E, and both determine the extent of excimer formation. The 6-fold and 7-fold enhancements of quantum yield in copolymers **4** and **5**, respectively, in the $f < 50\%$ composition region imply a dramatic reduction of f_E and the minimization of the denominator of equation (3).

Electroactive Properties

One of the possible applications of the rod-coil copolymers which have significantly enhanced solid state luminescence quantum efficiency compared to currently known π-conjugated polymers is in the development of light-emitting diodes which are based on charge injection electroluminescence.[3] A preliminary investigation of the electroactivity of some of the rod-coil copolymers **4** and **5** was done by cyclic voltammetry. Figure 15 shows the cyclic voltammograms (CVs) of the reduction of thin films of copolymers **4e** and **4h** and the conjugated polymer **1**. The one-electron reduction of **1** and the copolymers is seen to be quasi-reversible. The reduction potential of the copolymers **4e** and **4h** is similar to that of **1** which is -1.86 V (vs SCE). These results suggests that electron injection into thin films of the copolymers can be made from electrodes. The CVs of the oxidation process also showed that the copolymers can be oxidized by charge injection, however, the oxidation was not reversible, similar to the conjugated polymer **1**.[39,40] Similar results were obtained with selected copolymers **5**. The preferential stability of these rod-coil copolymers to reduction rather than oxidation suggests that the

materials would be better electron transporting media than hole transport in accord with the electron-deficient nature of the benzobisthiazole ring in these copolymers and homopolymers. These preliminary results demonstrate the electroactivity of the rod-coil copolymers which together with their efficient solid state luminescence make this class of macromolecular materials promising for exploring light-emitting diodes.

CONCLUSIONS

Our exploration of the rod-coil copolymer chain architecture as a structural motif for organizing macromolecular materials at the supramolecular level has revealed that the "supramolecular engineering" approach to solid state photophysical properties is feasible. The specific photoactive rod-coil copolymer systems that we investigated have allowed us to demonstrate the synthetic control of supramolecular structure and morphology which in turn regulates solid state photophysical properties such as luminescence (and non-radiative energy transfer[16c]). Our observations suggest that rod-coil copolymers containing *conjugated rigid rodlike segments* and inactive coillike segments, at rod compositions of $f<0.5$, represent electroactive and photoactive nanocomposite materials in which photophysical properties are significantly enhanced compared to the "bulk" electroactive and photoactive *rodlike homopolymers*. These rod-coil copolymers are excellent model systems for exploring theoretical ideas and models of photophysical processes in macromolecular materials, for example the effects of spatial confinement of chromophores, distribution of π-conjugation length, chain topology, supramolecular structure, and interchromophore interactions on electronic, photophysical, and nonlinear optical properties.

ACKNOWLEDGMENTS

This research was supported by the Office of Naval Research and in part by the National Science Foundation (Grant CTS-9311741), the Center for Photoinduced Charge Transfer (Grant CHE-9120001), and a Link Foundation Fellowship to J.A.O.

REFERENCES

1. (a) Aldissi, M., Ed. *Intrinsically Conducting Polymers: An Emerging Technology*, Kluwer Academic Publishers, Dordrecht, The Netherlands, 1993; (b) Bredas, J. L.; Chance, R. R. Eds. *Conjugated Polymeric Materials: Opportunities in Electronics, Optoelectronic, and Molecular Electronics*, Kluwer Academic Publishers: Dordrecht, Netherland, 1990. (c) Skotheim, T. A., Ed. *Handbook of Conducting Polymers*; Marcel Dekker: New York, 1986.
2. (a) Jenekhe, S. A., Ed. *Macromolecular Host-Guest Complexes: Optical, Optoelectronics, and Photorefractive Properties and Applications*, Materials Research Society: Pittsburgh, PA, 1992. (b) Marder, S. R.; Sohn, J. E.; Stucky, G. D., Eds. *Materials for Nonlinear Optics: Chemical Perspectives*, American Chemical Society: Washington, DC, 1991; (c) Hornak, L. A., Ed. *Polymer for Lightwave and Intergrated Optics: Technology and Applications*, Marcel Dekker: New York, 1992.
3. (a) Burroughes, J. H; Bradley, D. D. C.; Brown, A. R.; Marks, R. N.; Mackay, K.; Friend, R. H.; Burn, P. L.; Holmes, A. B. *Nature* **1990**, *347*, 539-541. (b) Bradley, D. D. C. *Adv. Mater.* **1992**, *4*, 756-758.
4. Miller, J. S. *Adv. Mater*. **1993**, *5*, 587; *ibid*, **1993**, *5*, 671.
5. (a) Law, K-Y. *Chem. Rev.* **1993**, *93*, 449-486. (b) Borsenberger, P. M.; Weiss, D. S. in *Handbook of Imaging Materials,* Diamond, A. S. Ed.; Marcel Dekker; New York: 1991, p.379-446. (c) Pai, D. M.; Springett, B. E. *Rev. Mod. Phys.* **1993**, *65*, 163-211.
6. Antoniadis, H.; Abkowitz, M. A.; Osaheni, J. A.; Jenekhe, S. A.; Stolka, M. *Synth. Metals* **1993**, *60*, 149-157.
7. (a) Jenekhe, S. A.; Osaheni, J. A.; Meth, J. S.; Vanherzeele, H. *Chem. Mater.* **1992**, *4*, 683-687. (b) Osaheni, J. A.; Jenekhe, S. A.; Vanherzeele, H.; Meth, J. S. *J. Phys. Chem.* **1992**, *96*, 2830-2836. (c) Agrawal, A. K.; Jenekhe, S. A.; Vanherzeele, H.; Meth, J. S. *J. Phys. Chem.* **1992**, *96*, 2837-2843. (d) Vanherzeele, H.; Meth, J. S.; Jenekhe, S. A.; Roberts, M. F. *J. Opt. Am.* **1992**, *B9*, 524-533.

8. Osaheni, J. A.; Jenekhe, S. A. *Macromolecules* **1994**, *27*, 739-741.

9. (a) Jenekhe, S. A.; Osaheni, J. A. *Science* **1994**, *265*, 765-768. (b) Osaheni, J. A.; Jenekhe, S. A.; in preparation.

10. (a) Osaheni, J. A.; Jenekhe, S. A.; Perlstein, J. *Appl. Phys. Lett.* **1994**, *64*, 3112-3114. (b) Osaheni, J. A.; Jenekhe, S. A.; Perlstein, J. *J. Phys. Chem.* **1994**, 98,12727-12736.

11. McGrath, K. P.; Fournier, M. J.; Mason, T. L.; Tirrell, D. A. *J. Am. Chem. Soc*. **1992**, *114*, 727-733.

12. Frechet, J. M. J. *Science* **1994**, *263*, 1710-1715.

13. Stupp, S. I.; Son, S.; Lin, H. C.; Li, L. S. *Science* **1993**, *259*, 59-63.

14. Chan, W.-K.; Chen, Y.; Peng, Z.; Yu, L. *J. Am. Chem. Soc.* **1993**, *115*, 11735-11743.

15. Roberts, M. F.; Jenekhe, S. A.; Cameron, A.; McMillan, M.; Perlstein, J. *Chem. Mater.* **1994**, *6*, 658-670.

16. (a) Jenekhe, S. A.; Osaheni, J. A. *Chem. Mater.* **1994**, 6, 1906-1909. (b) Jenekhe, S. A.; Osaheni, J. A. *Bull. Am. Phys. Soc.* **1994**, 39(1), 505. (c) Yang, C. J.; Jenekhe, S. A. *Supramolecular Sci*. **1994**, in press.

17. Radzilowski, L. H.; Wu, J. L.; Stupp, S. I. *Macromolecules* **1993**, 26, 879-882.

18 (a) Osaheni, J. A.; Jenekhe, S. A. *Chem. Mater.* **1992**, *4*, 1282-1290. (b) Osaheni, J. A.; Jenekhe, S. A. *Macromolecules* **1993**, *26*, 4726-4728. (c) *ibid*, in press.

19. (a) Jenekhe, S. A.; Johnson, P. O.; Agrawal, A. K. *Macromolecules* **1989**, *22*, 3216-3222. (b) Jenekhe, S. A.; Johnson, P. O.*Macromolecules* **1990**, *23*, 4419-4429.

20. Eaton, D. F. *Pure & Appl. Chem.* **1988**, *60*, 1107-1114.

21. (a) Guilbault, G. G. Ed. *Practical Fluorescence*; Marcel Dekker, Inc.: New York, 1990; Chapter 1. (b) Demas, J. N.; Crosby, G. A. *J. Phys. Chem.* **1971**, *75*, 991-1024.

22. Silverstein, R. M.; Bassler, G. C.; Morrill, T. C. *Spectrometric Identification of Organic Compounds*, 4th Edition; Wiley: New York, 1981; Chapter 3.

23. Shen, D. Y.; Hsu, S. C. *Polymer* **1982**, *23*, 969-963.

24. Gupta, R. R. Ed. *Physical Methods in Heterocyclic Chemistry*; Wiley: New

York, 1984; p.45.

25. Koenig, J. C. *Spectroscopy of Polymers*; American Chemical Society: Washington, DC, 1992.
26. Wolfe, J. F. in *Encylopaedia of polymer Science and Engineering*, Wiley: New York, 1988; vol. 11, p601-635.
27. Odian, G. *Principles of Polymerization*, 2nd Ed.; Wiley-Interscience: New York 1981; p.143.
28. Randall, J. C., Ed. *NMR and Macromolecules: Sequence, Dynamic and Domain Structure*; American Chemical Society: Washington, DC, 1984.
29. Petsch, E.; Clerc, T.; Seibl, J.; Simon, W. *Spectral Data for Structure Determination of Organic Compounds*, 2nd Edition, Springer-Verlag: New York, 1989; p120-161.
30. Flory, P. J. *Macromolecules* **1978**, *11*, 1138-1141.
31. Allen, S. R.; Farris, R. J.; Thomas, E. L. *J. Mater. Sci.* **1985**, *20*, 4583-4592.
32. Craig, G. S. W.; Cohen, R. E.; Schrock, R. R.; Silbey, R. J.; Puccetti, G.; Ledoux, I.; Zyss, J. *J. Am. Chem. Soc*. **1993**, *115*, 860-867.
33. Rauscher, U.; Bassler, H.; Bradley, D. D. C.; Hennecke, M. *Phys. Rev. B* **1990**, *42*, 9830-9836.
34. (a) Spano, F. C.; Mukamel, S. *Phys. Rev. Lett.* **1991**, *66*, 1197-1200. (b) Spano, F. C.; Kuklinski, J. R.; Mukamel, S. *J. Chem. Phys*. **1991**, *94*, 7534-7544.
35. Tsutsui, T.; Saito, S. in ref. 1a, p123-134.
36. Birks, J. B.; Dyson, D. J.; Munro, I. H. *Proc. Royal. Soc. London A* **1963**, *275*, 575-588.
37. Johnson, G. E. *J. Chem. Phys.* **1975**, *62*, 4697-4709.
38. Fox, M. A.; Britt, P. F. *Macromolecules* **1990**, *23*, 4533-4542.
39. DePra, P. A.; Gaudiello, J. G.; Marks, T. J. *Macromolecules* **1988**, *21*, 2295-2297.
40. Osaheni, J. A.; Jenekhe, S. A. *Chem. Mater.*, in press.

Table 1. Physical Properties of Copolymers **4** and **5** and homopolymers **1-3**.

Composition f (Mole%)	Intrinsic Viscosity [η][a] (dL/g)		Thermal Stability[b] (°C)	
	(4)	(5)	(4)	(5)
0 (2)	3.3	3.3	450	450
5 (a)	4.5	3.5	452	450
10 (b)	5.6	3.8	460	452
20 (c)	5.3	4.2	454	452
30 (d)	4.2	3.4	458	455
40 (e)	6.7	4.8	466	455
50 (f)	4.1	3.6	460	457
65 (g)	4.3	4.5	463	456
80 (h)	6.5	4.6	477	460
100 (1, 3)	32.0	5.0	720	560

a. in methanesulfonic acid at 30±0.5 °C.

b. Onset of thermal decomposition in N_2 at 10 °C/min.

Table 2. Time-resolved PL decay dynamics parameters for copolymers **4** and conjugated polymer **1** excited at $\lambda = 380$ nm.

Composition	Monitoring Wavelength λ (nm)	Lifetime t (ns)	Amplitude (%)
4a	486	0.62	65
4b	501	0.72	62
4c	502	0.90	80
4e	536	0.57	70
4h	550	0.52	38
1	560	0.50	30

Figure Captions

Figure 1. Chain structure of a rod (B)-Coil (A) segmented copolymer (a) and its three possible ordered (b), semi-ordered (c) and disordered (d) self-assembling supramolecular structures and morphologies.

Figure 2. ^{1}H NMR integration versus feed composition of copolymers **4a-4h**.

Figure 3. Probability distribution of block sizes in **4e**.

Figure 4. Comparison of total -AA- sequence obtained from ^{1}H NMR integration and the probability distribution model: (1) ^{1}H NMR integration; (2) Model.

Figure 5. Probability distribution of block sizes in copolymer **4** at different compositions *f*.

Figure 6. Model of the supramolecular structure and morphology of the rod-coil copolymers at one composition *f*.

Figure 7. Optical absorption spectra of thin films of copolymers **4** and pure PBZT. (1), PBZT; (2), **4h**; (3), **4f**; (4), **4e**; (5), **4c**; (6), **4a**.

Figure 8. Absorption and emission λ_{max} as a function of copolymer composition of **4**.

Figure 9. Optical absorption spectra of thin films of copolymers **5** and PBTPV: (1), PBTPV; (2), **5h**; (3), **5e**; (4), **5d**; (5), **5c**; (6), **5b**; (7), **5a**.

Figure 10. Absorption and emission λ_{max} versus composition of copolymers **5**.

Figure 11. Photoluminescence spectra of copolymers **4** and PBZT: (1), PBZT; (2), **4h**; (3), **4e**; (4), **4c**; (5), **4a**.

Figure 12. Photoluminescence spectra of copolymers **5** and PBTPV: (1), **5a**; (2), **5b**; (3), **5c**; (4), **5f**; (5), PBTPV.

Figure 13. Photoluminescence quantum efficiency versus composition of copolymers **4** and **5**.

Figure 14. Time-resolved PL decay dynamics of copolymers **4**: (1), **4c**; (2), **4b**; (3), **4d**; (4), **4h**.

Figure 15. Reduction cyclic voltamogram of copolymers **4** and PBZT at 20 mV/s: (1), **4e**; (2), **4h**; (3), PBZT.

Chart I

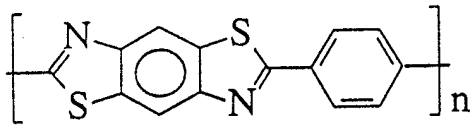

1. PBZT

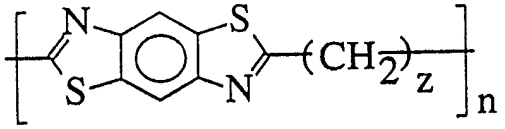

2. PBTC10, z = 10

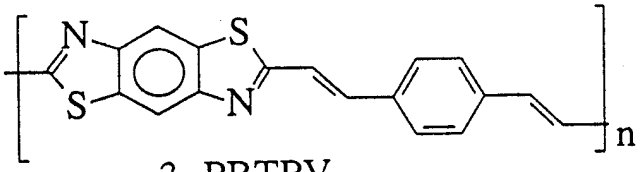

3. PBTPV

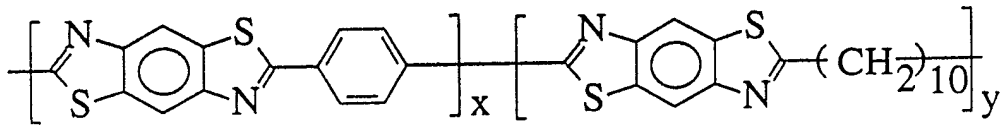

4. PBZT-*co*-PBTC10

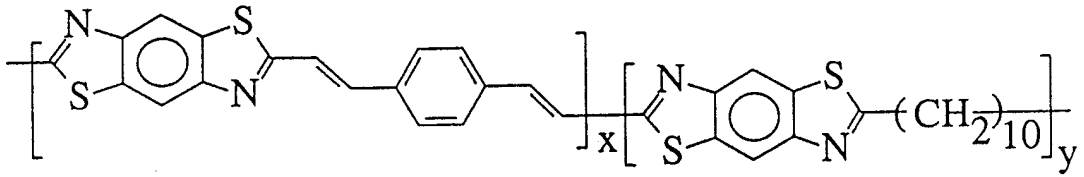

5. PBTPV-*co*-PBTC10

a. x/(x+y) = 5%
b. " = 10%
c. " = 20%
d. " = 30%
e. " = 40%
f. " = 50%
g. " = 65%
h. " = 80%

Scheme I

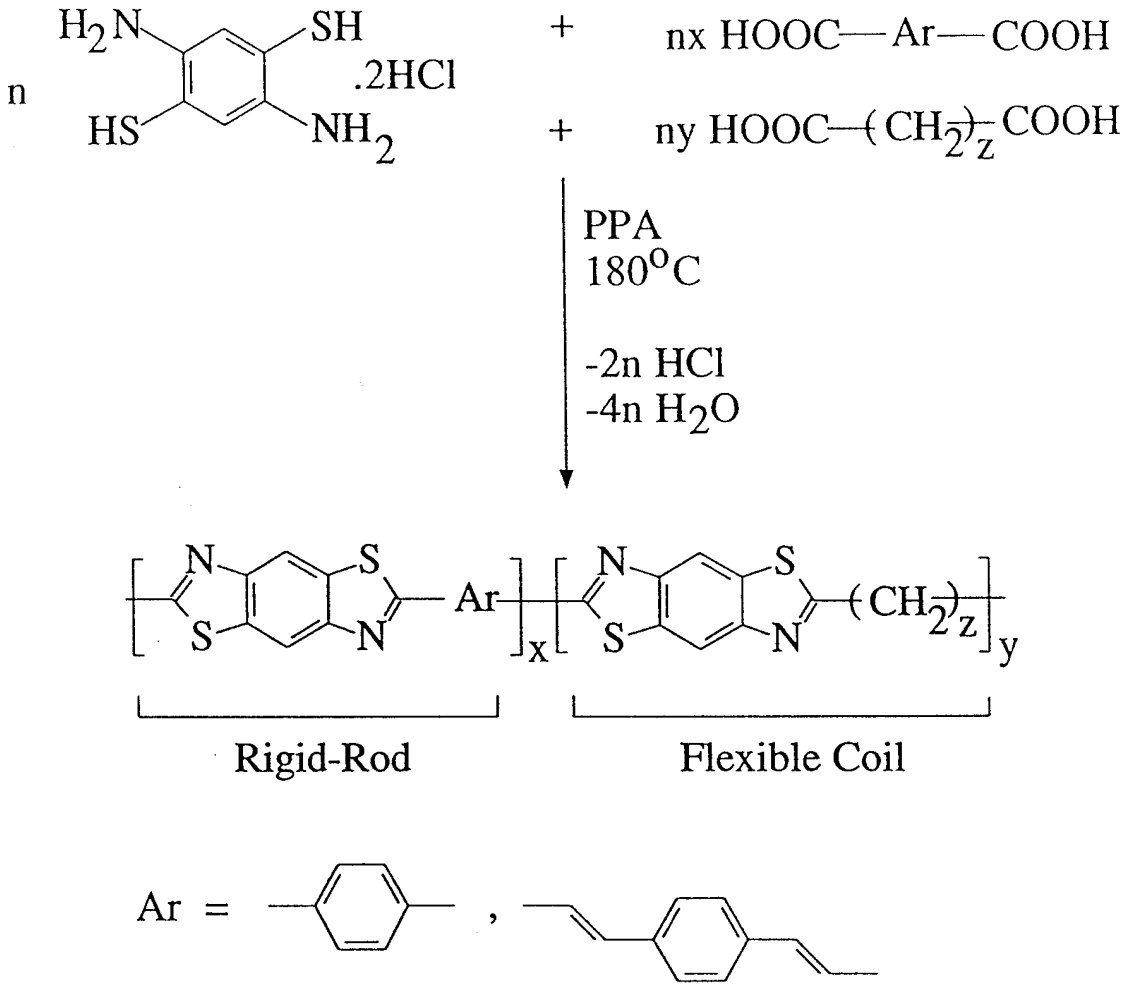
n
H_2N
SH
.2HCl
HS
NH_2
+ nx HOOC—Ar—COOH
+ ny HOOC—$(CH_2)_z$—COOH
PPA
180°C
-2n HCl
-4n H_2O
N
S
Ar
x
y
$(CH_2)_z$
Rigid-Rod
Flexible Coil

Ar =

Fig. 1

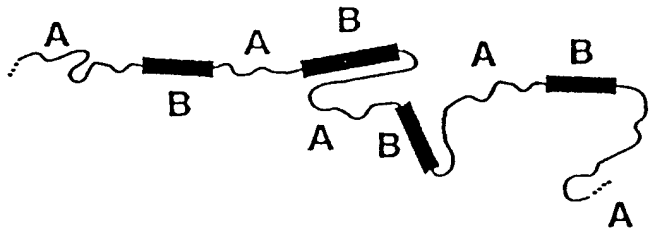

a. Rod(B)-Coil(A) Copolymer

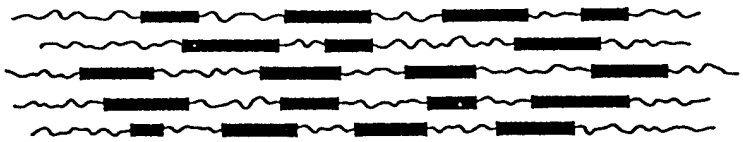

b. Ordered

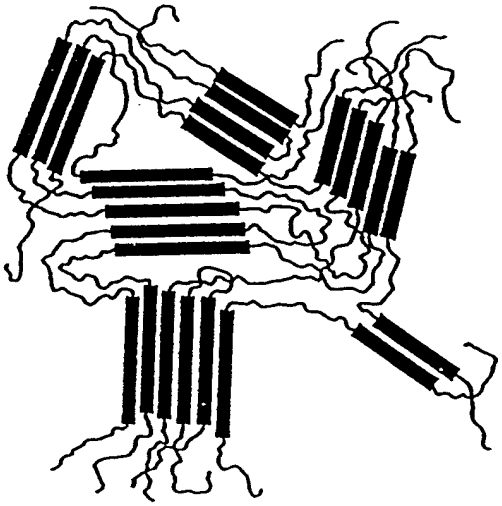

c. Semi-Ordered

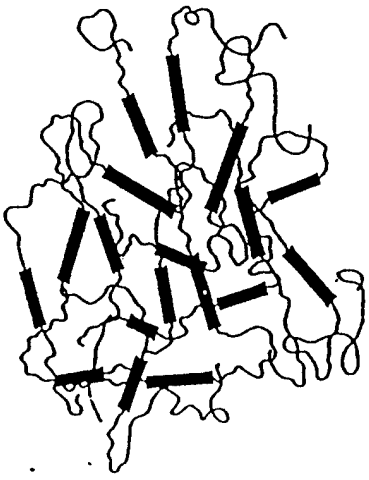

d. Disordered

Fig. 3 (2)

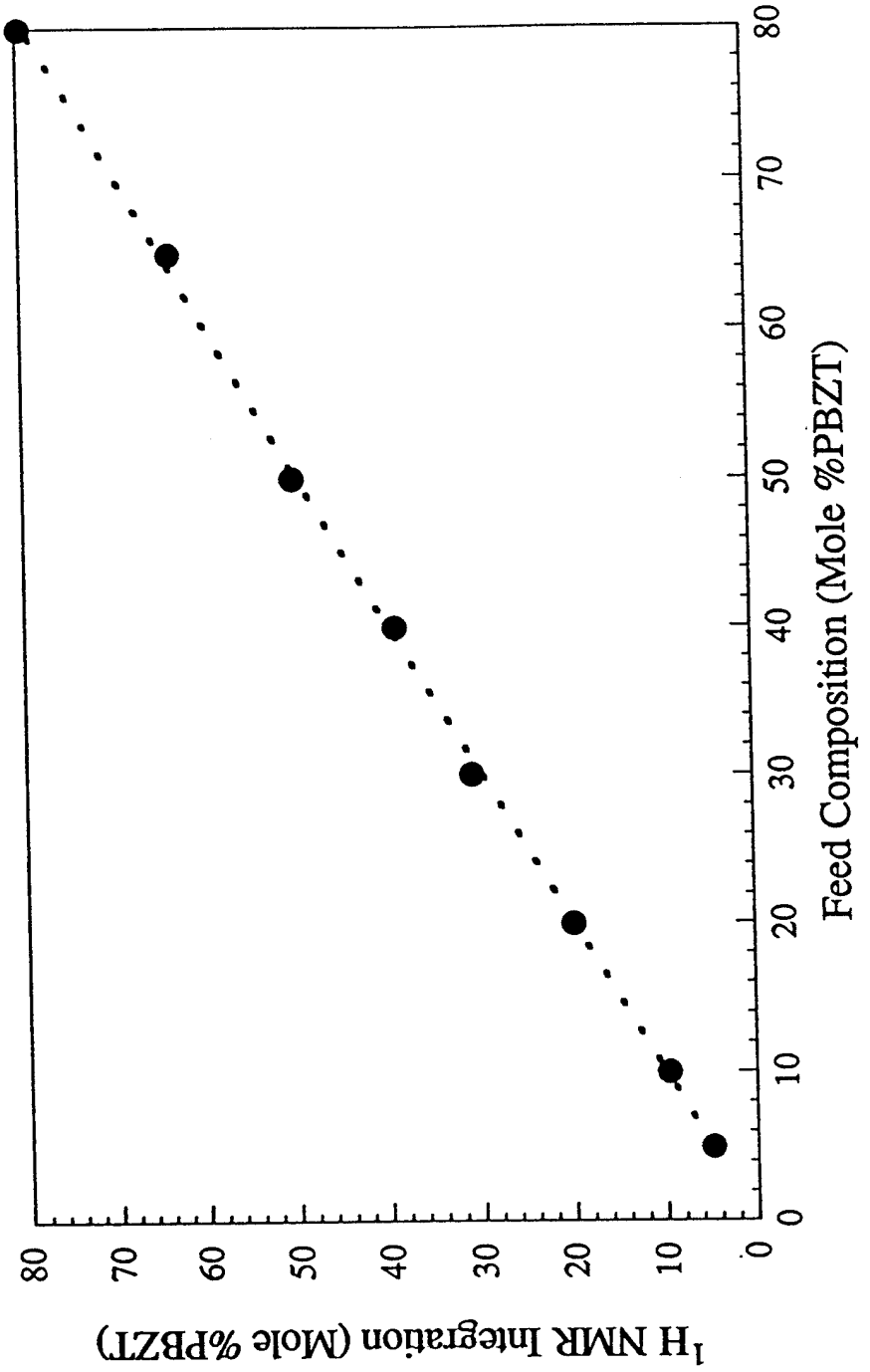
^{1}H NMR Integration (Mole %PBZT)
0
10
20
30
40
50
60
70
80
Feed Composition (Mole %PBZT)
0
10
20
30
40
50
60
70
80

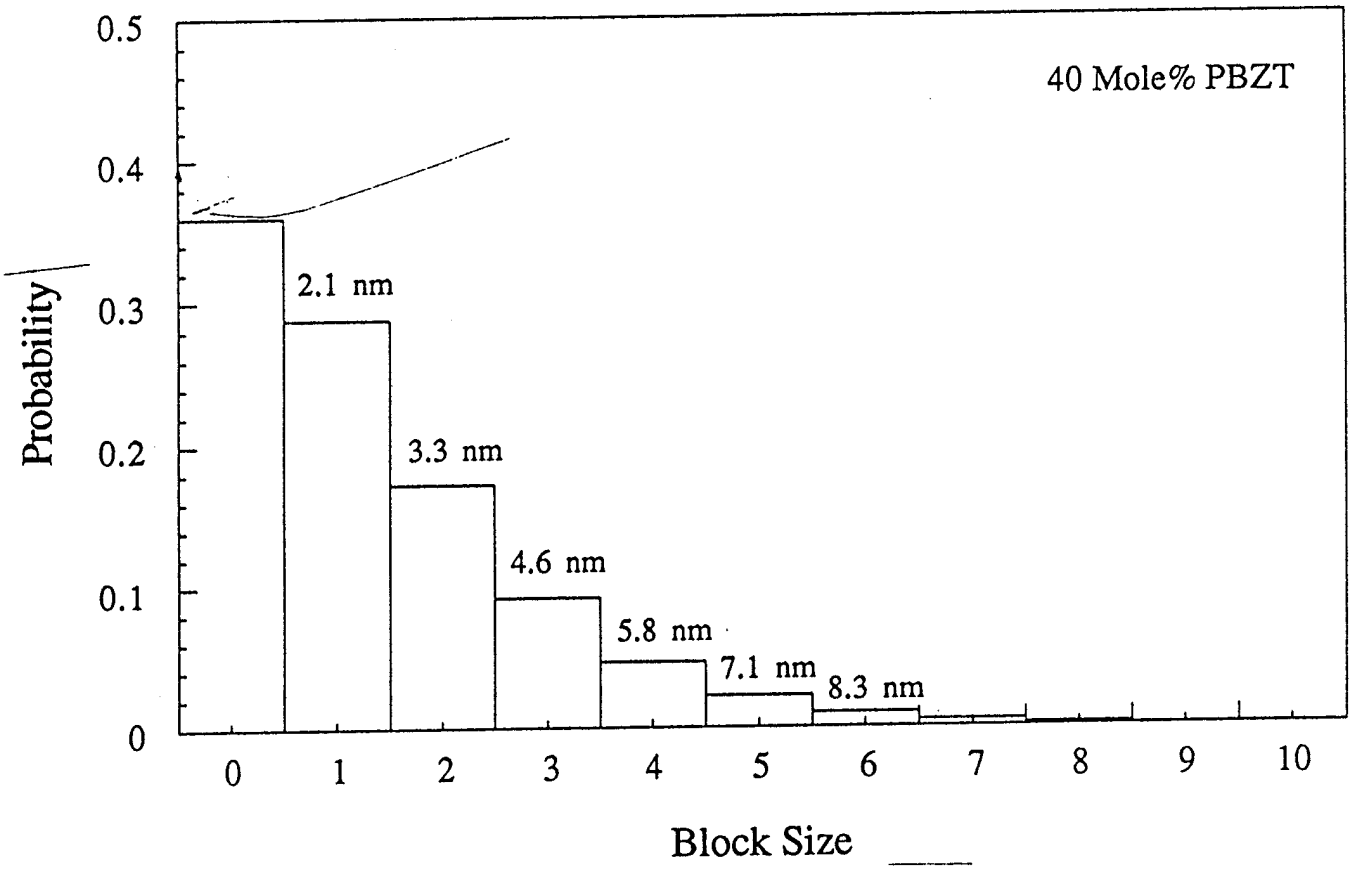
40 Mole% PBZT
Probability
0.5
0.4
0.3
0.2
0.1
0
2.1 nm
3.3 nm
4.6 nm
5.8 nm
7.1 nm
8.3 nm
0
1
2
3
4
5
6
7
8
9
10
Block Size

Fig. 9

(3)

Fig. 4

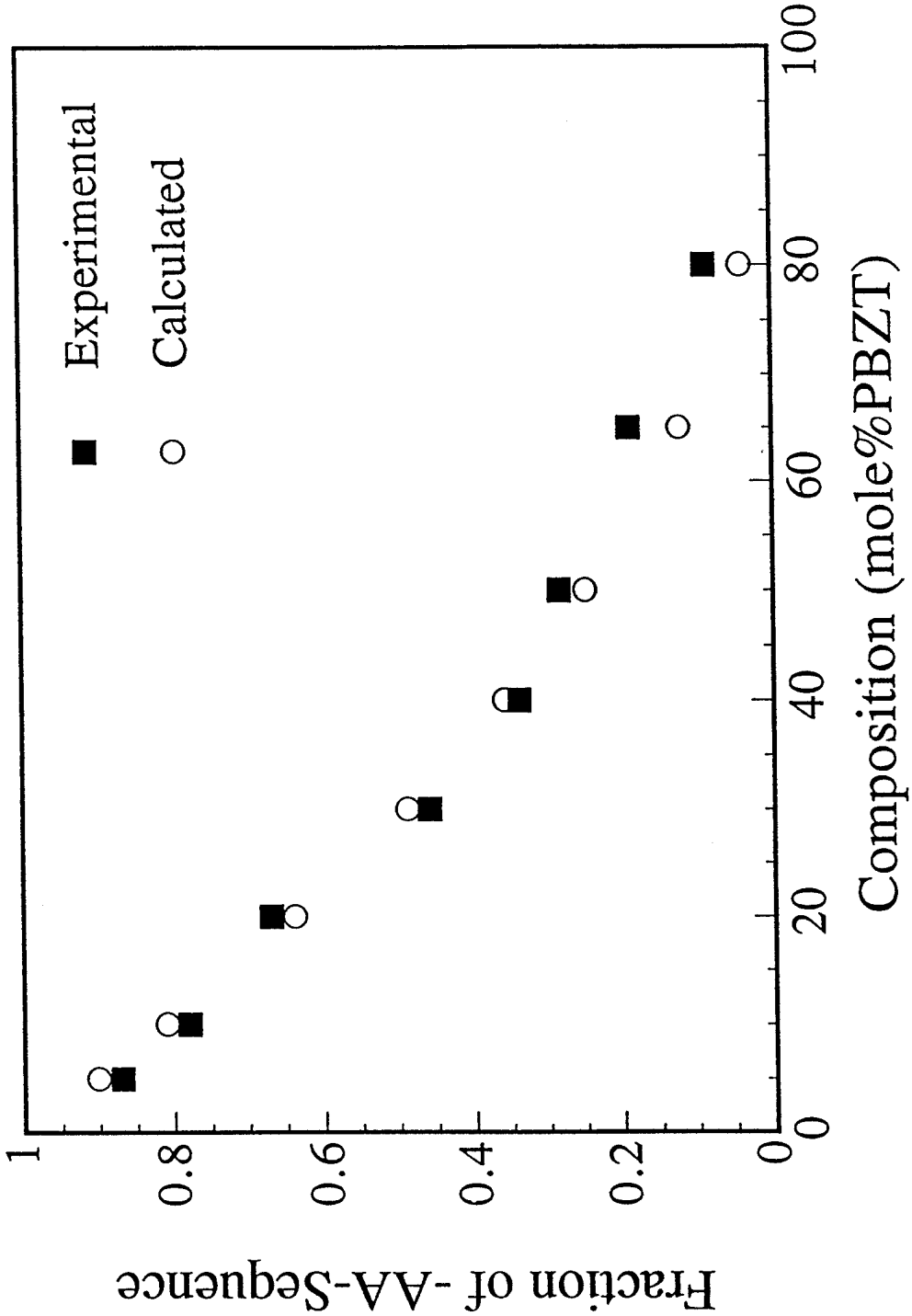
Experimental
Calculated
Fraction of -AA-Sequence
Composition (mole%PBZT)
0
0.2
0.4
0.6
0.8
1
0
20
40
60
80
100

Fig. 12
(5)

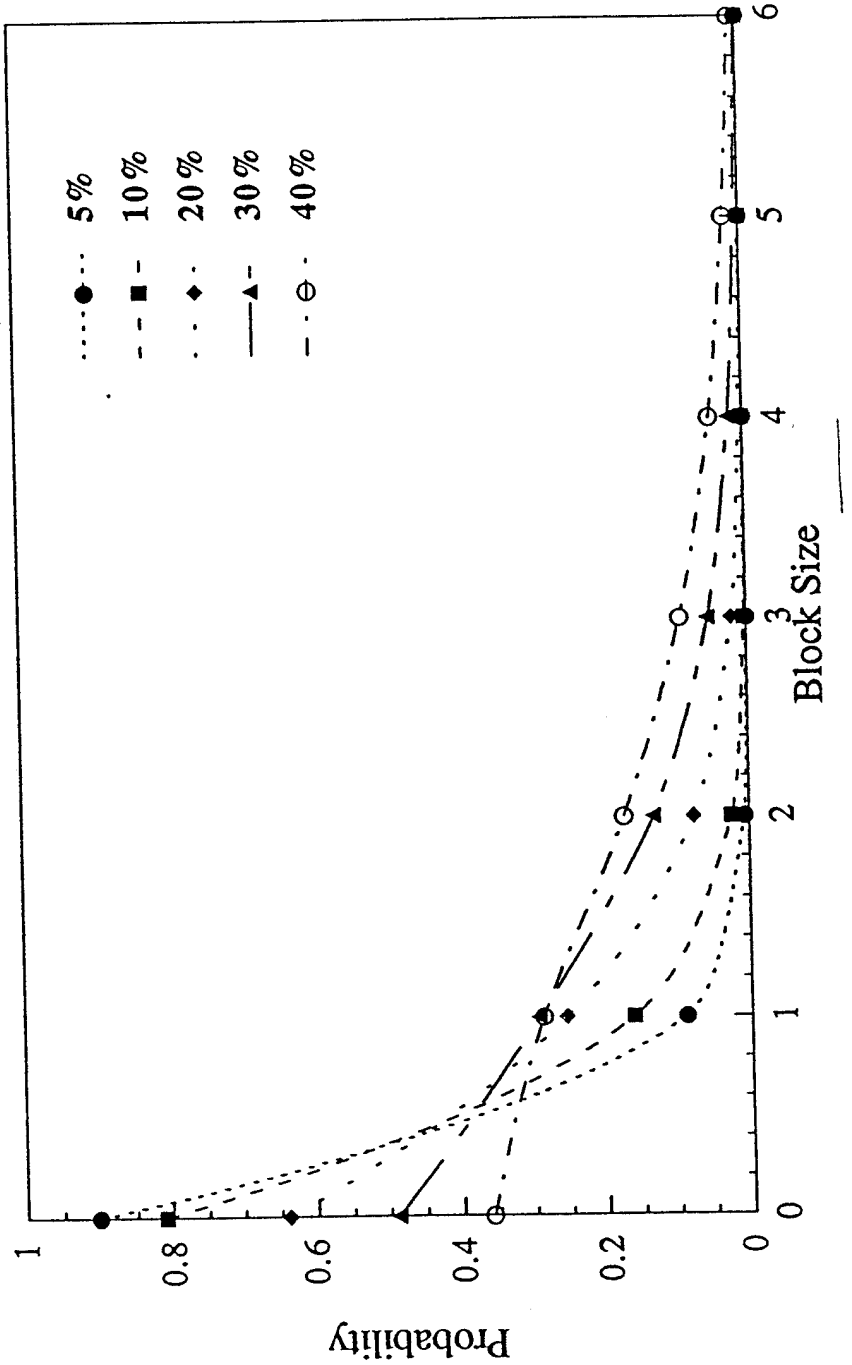

Fig. ~~17~~ (6)

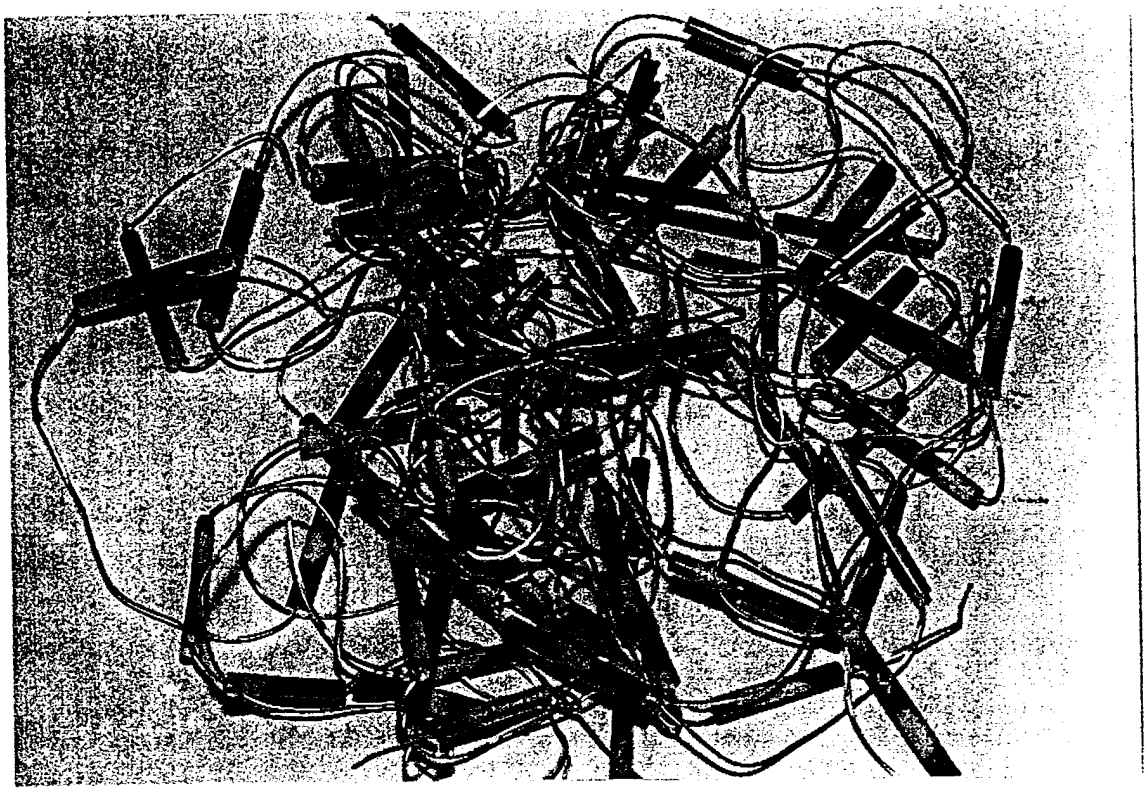

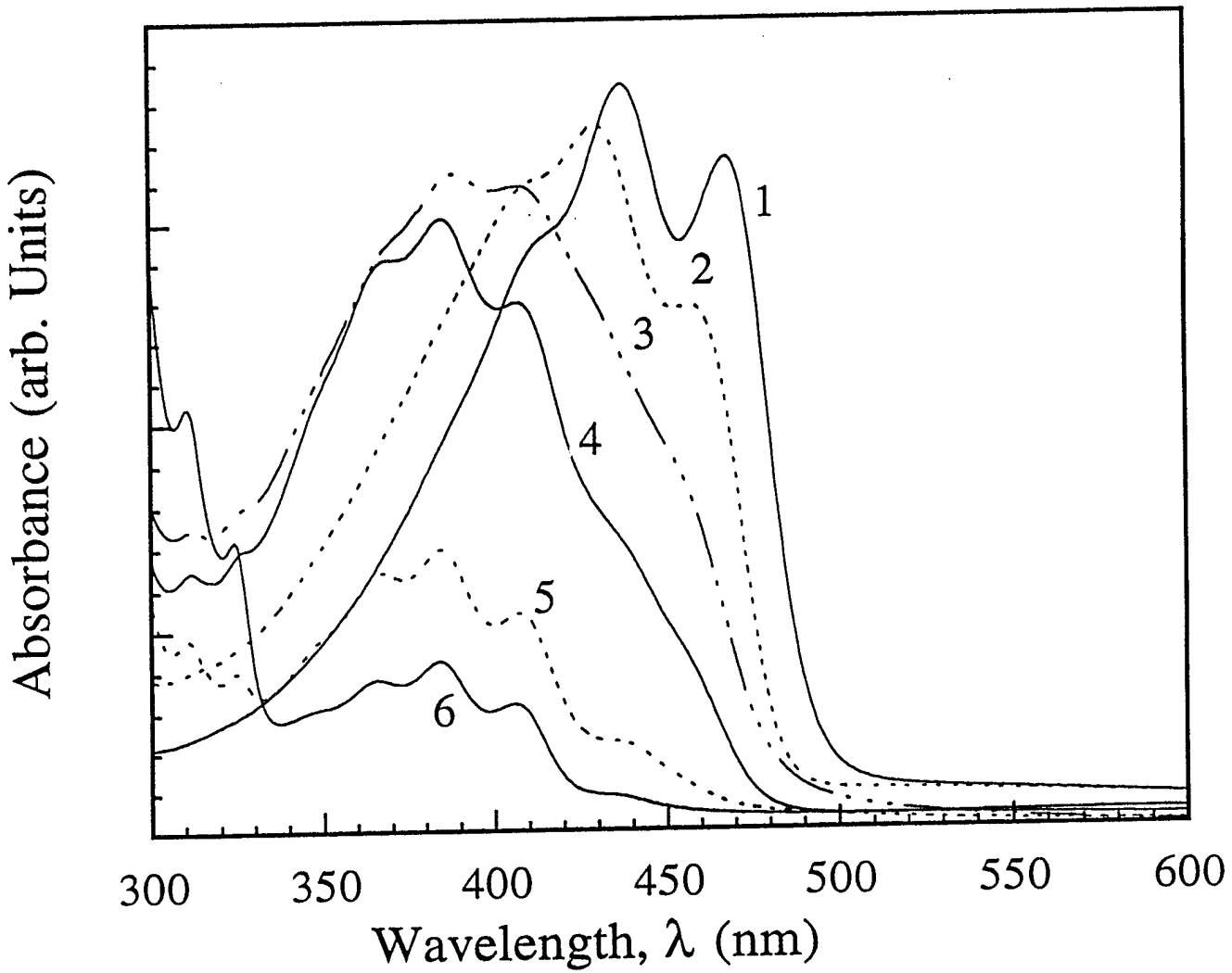
Absorbance (arb. Units)
1
2
3
4
5
6
300
350
400
450
500
550
600
Wavelength, λ (nm)

Fig. 18

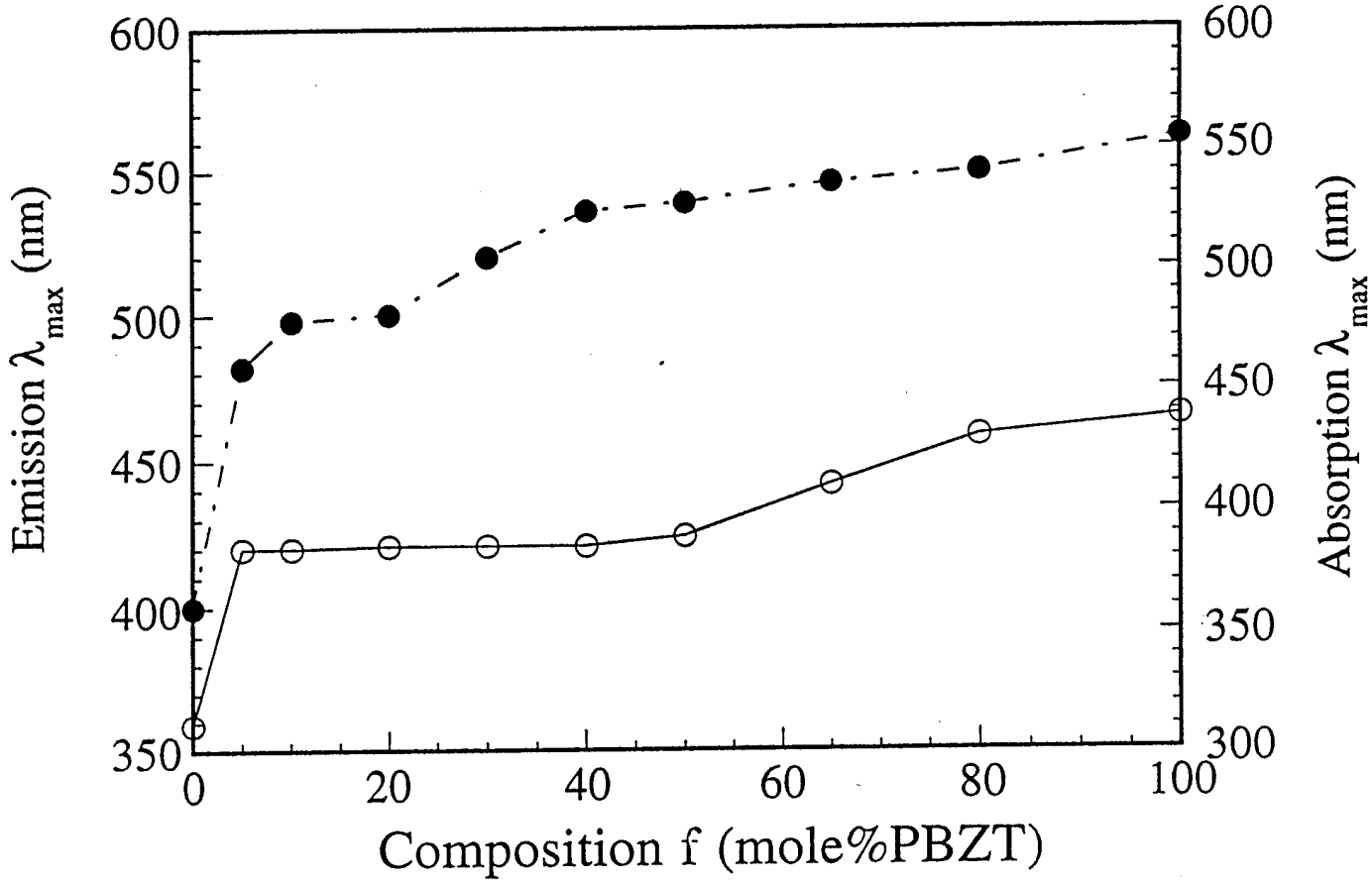
Emission λ_{max} (nm)
Absorption λ_{max} (nm)
Composition f (mole%PBZT)
600
550
500
450
400
350
300
0
20
40
60
80
100

Fig. 14

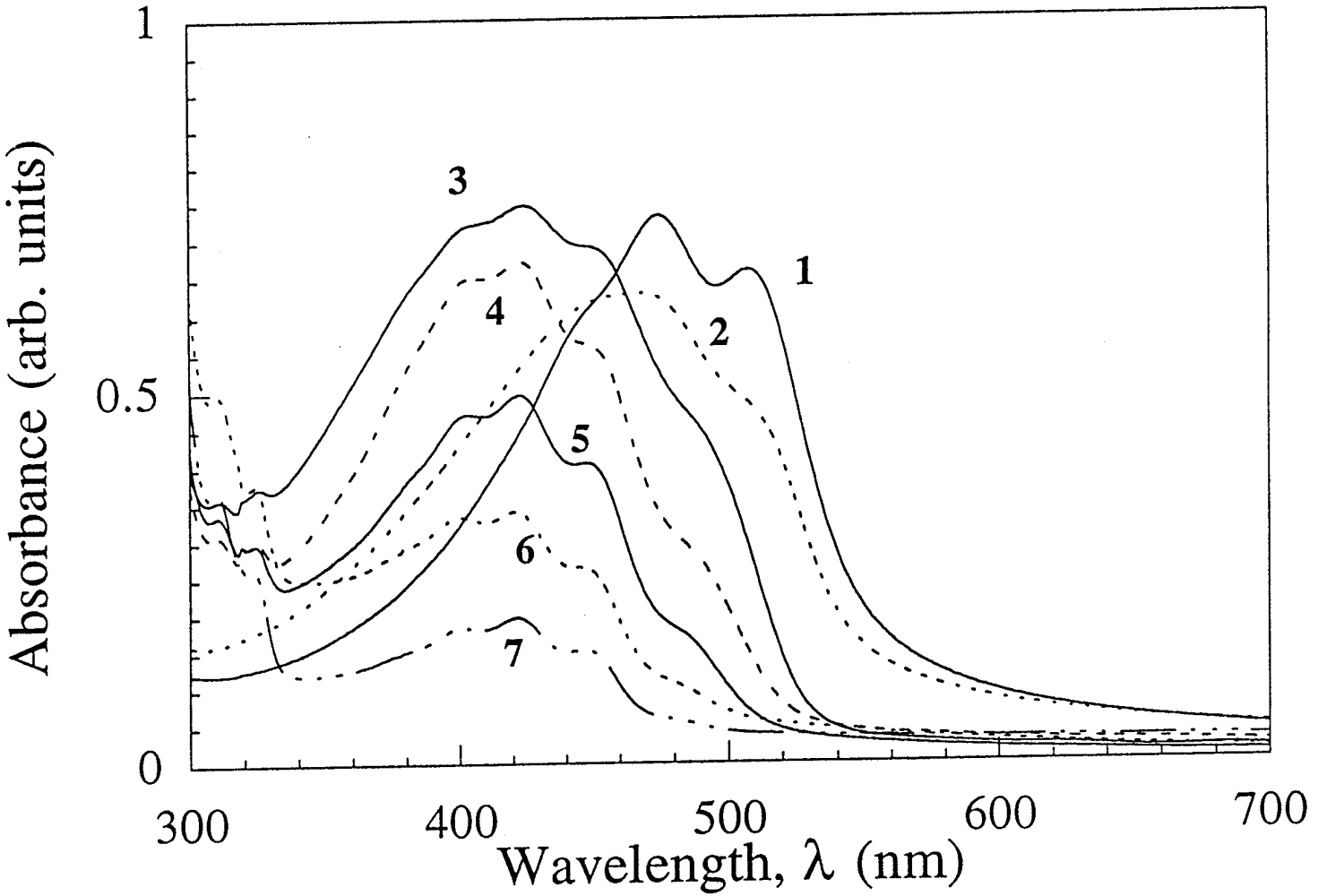
Absorbance (arb. units)
1
0.5
0
300
400
500
600
700
Wavelength, λ (nm)
1
2
3
4
5
6
7

Fig. 2a

9

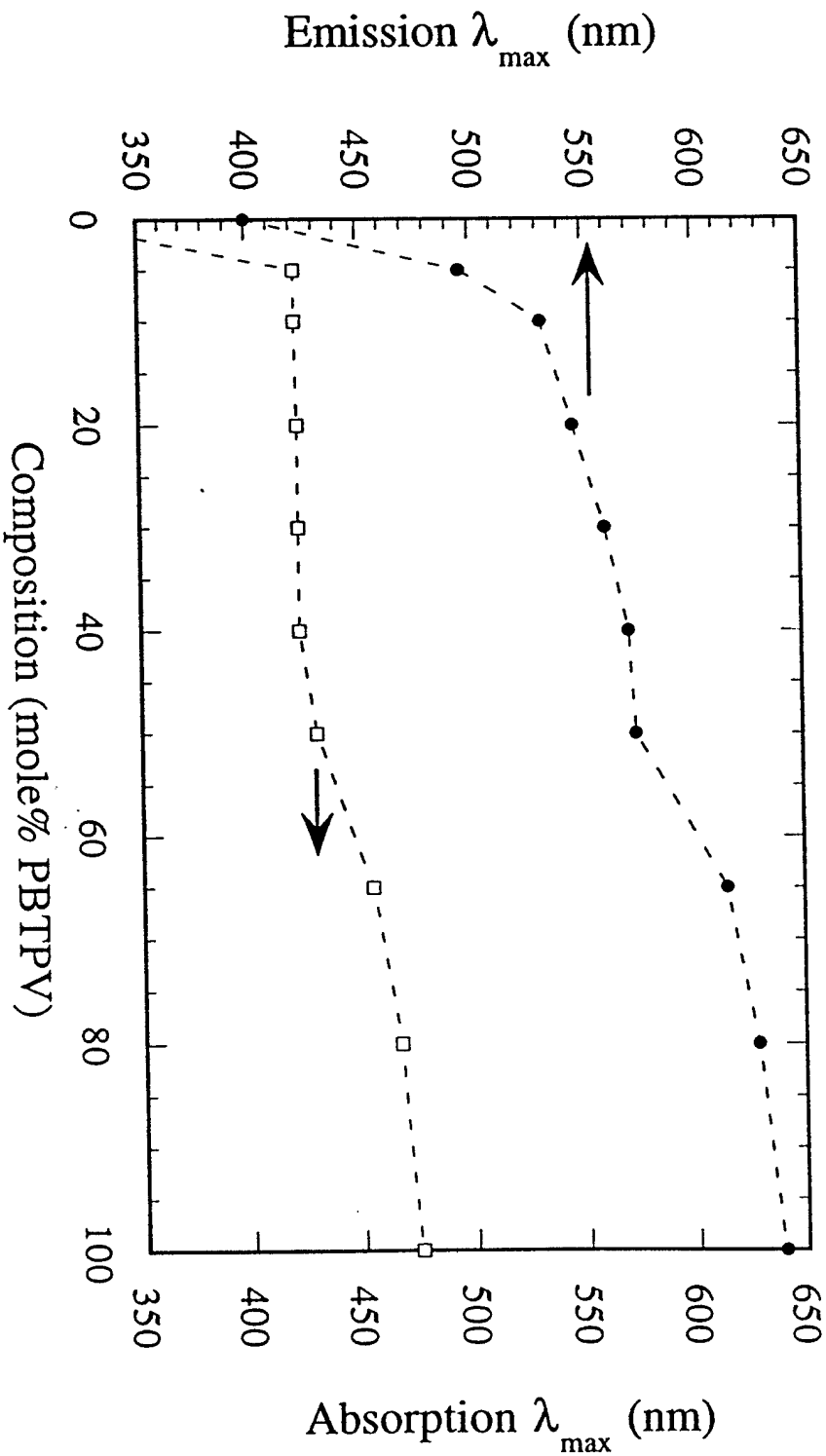
Emission λmax (nm)
350
400
450
500
550
600
650
0
20
40
60
80
100
Composition (mole% PBTPV)
Absorption λmax (nm)

Fig. 21

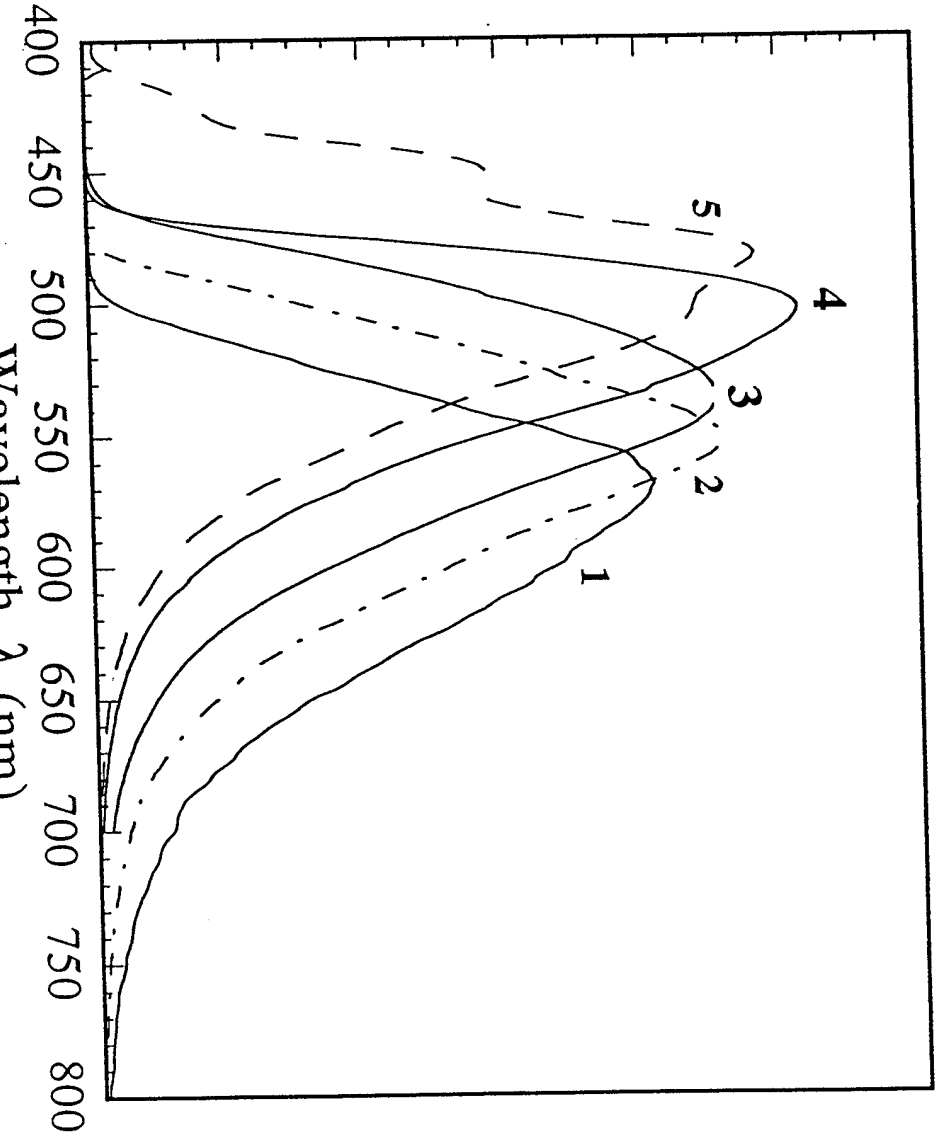
PL Intensity, (arb. units)
400
450
500
550
600
650
700
750
800
Wavelength, λ (nm)
1
2
3
4
5

Fig. 11

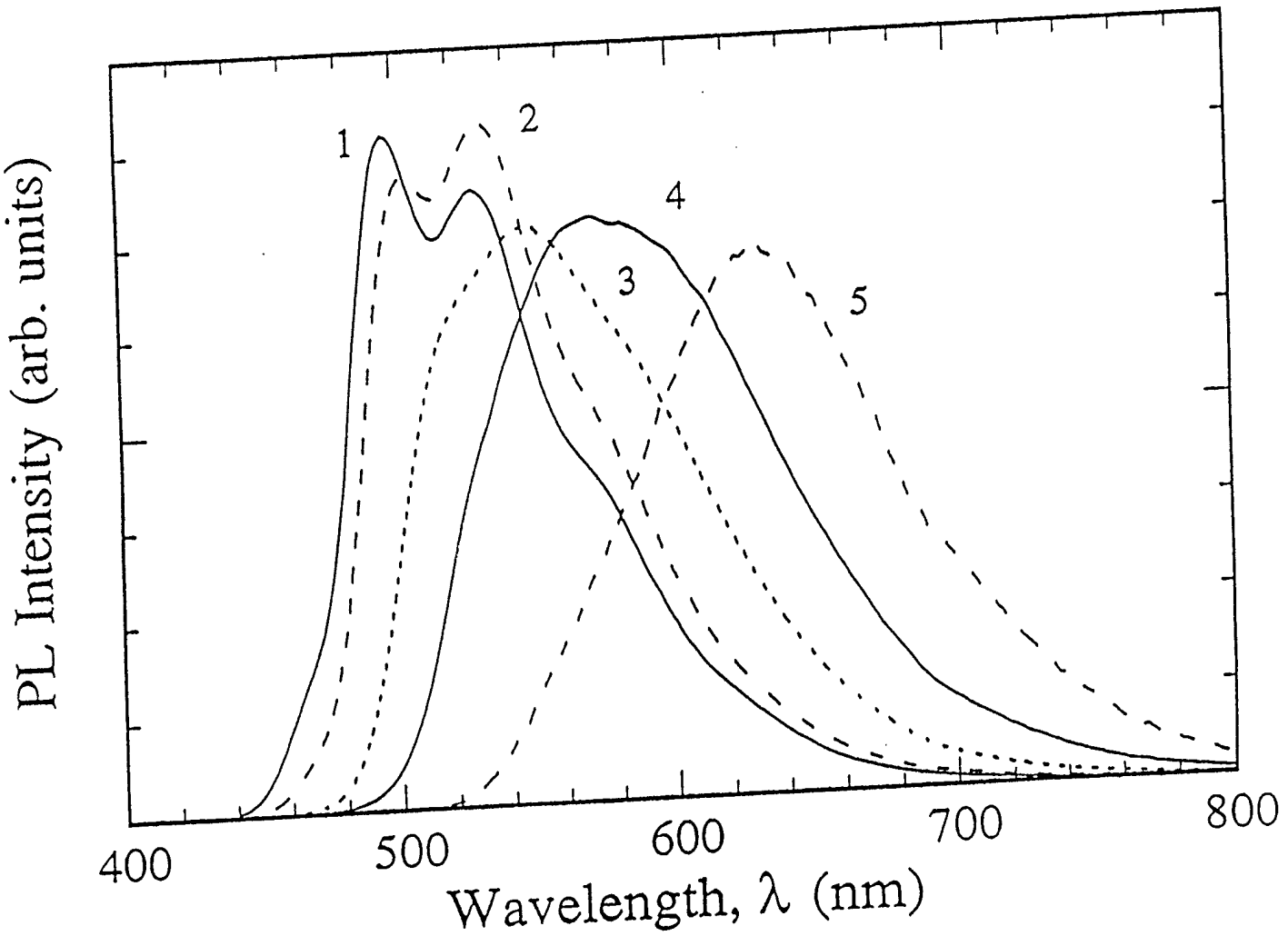

Figure 12. Photoluminescence spectra of copolymers **5** and PBTPV: (1), **5a**; (2), **5b**; (3), **5c**; (4), **5f**; (5), PBTPV.

Fig. 12

Fig. ~~24~~ 13

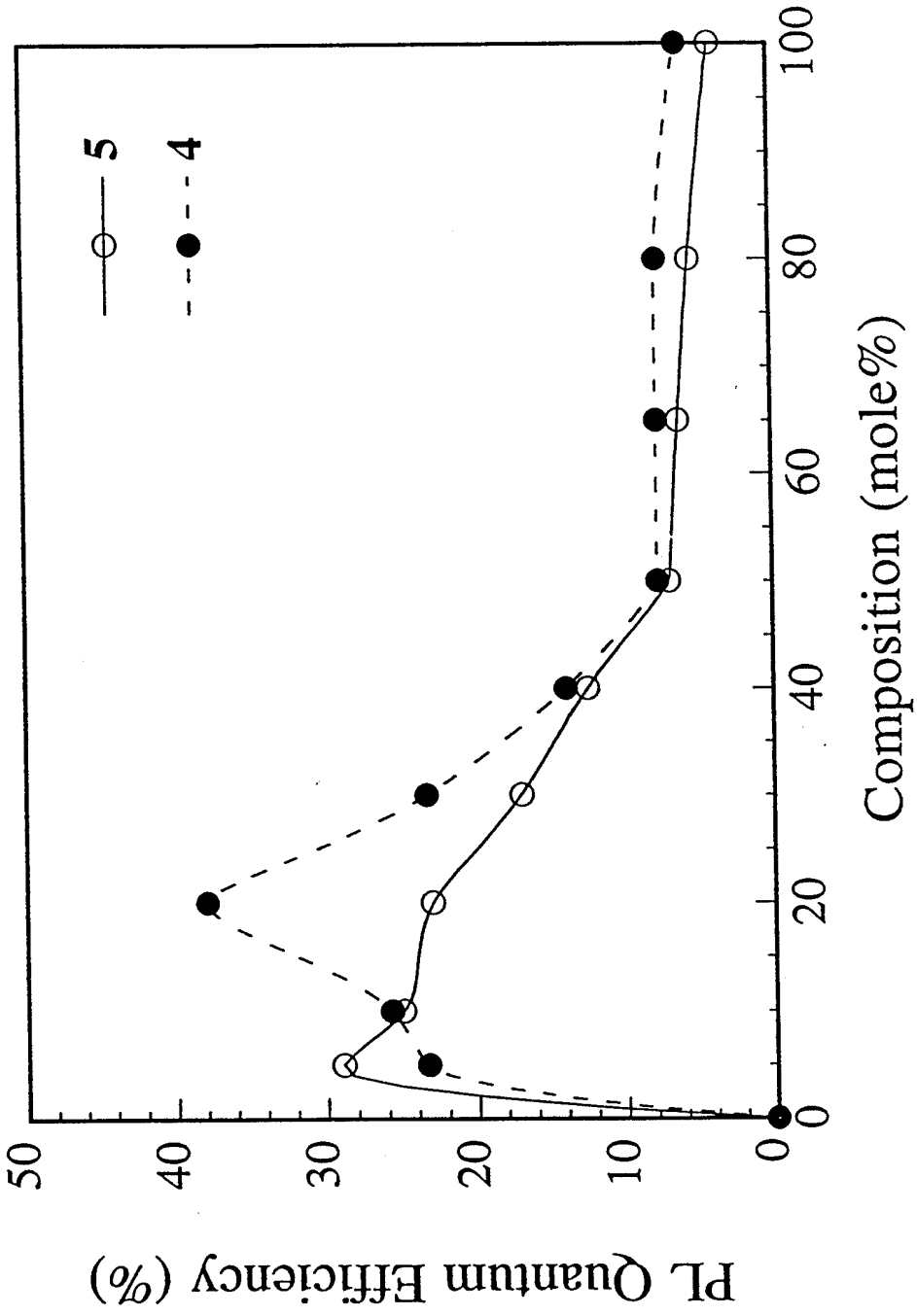
PL Quantum Efficiency (%)
50
40
30
20
10
0
0
20
40
60
80
100
Composition (mole%)
5
4

Fig. ~~25~~ 14

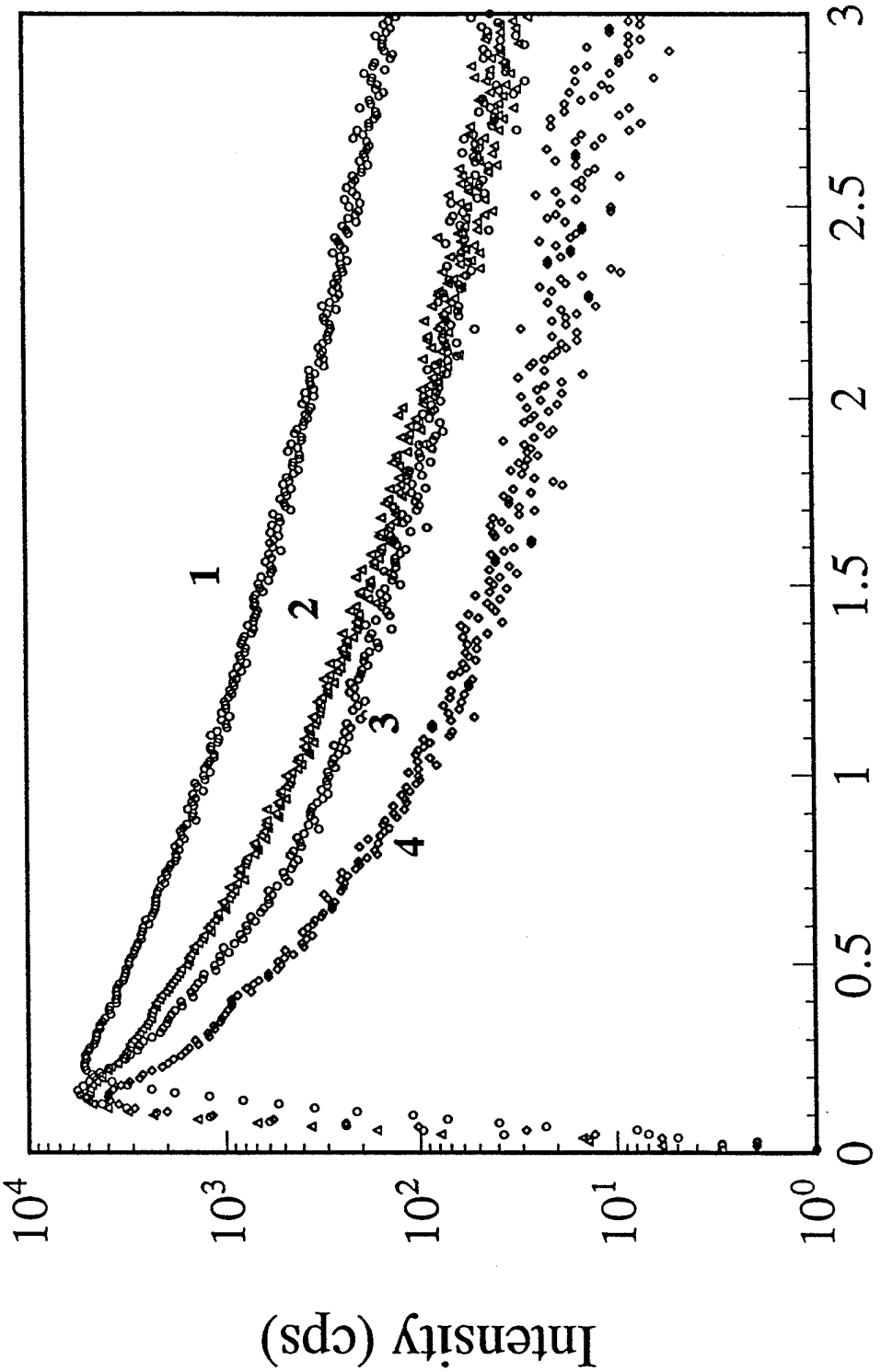

Fig. ~~26~~ 15

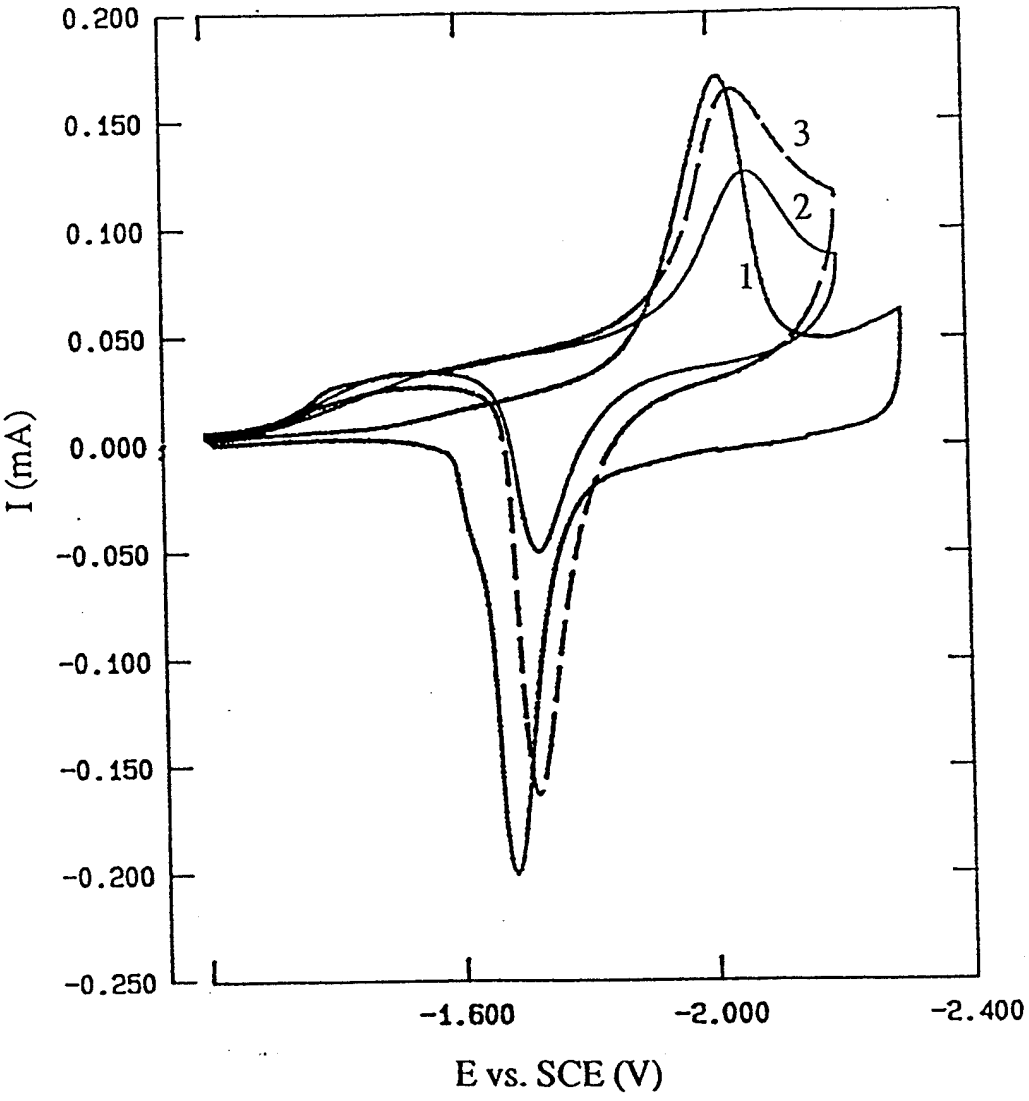
0.200
0.150
0.100
0.050
0.000
-0.050
-0.100
-0.150
-0.200
-0.250
I (mA)
1
2
3
-1.600
-2.000
-2.400
E vs. SCE (V)

Electroactive and Photoactive Rod-Coil Copolymers: Design, Synthesis, and Supramolecular Regulation of Photophysical Properties

John A. Osaheni† and Samson A. Jenekhe*

Department of Chemical Engineering and Center for Photoinduced Charge Transfer, University of Rochester, Rochester, New York 14627-0166.

SUPPLEMENTARY MATERIAL

Characterization. Figure S1 shows the ^{1}H NMR spectrum of **4f** in deuterated nitromethane-$AlCl_3$ which exemplifies the proton NMR spectra of the PBZT-*co*-PBTC10 copolymers **4**. The resonances and the number of protons corresponding to each resonance were in good agreement with the proposed structure of **4f**. Figure S2 shows the ^{1}H NMR spectrum of **5f** in deuterated nitromethane -$AlCl_3$ which is typical of the proton NMR spectra of the PBTPV-*co*-PBTC10 series of copolymers **5**. The number of resonances and their integration were in good agreement with the proposed structure **5f**. The ^{1}H NMR spectra of the other 7 copolymers **5** were also in excellent agreement with the proposed structures. The copolymer composition *f* of **5** was determined from the ratio of the *trans*-vinylene proton resonances (e.g. δ = 8.1 ppm) to the methylene proton resonances. Figure S3 shows the excellent agreement between the copolymer compositions determined from NMR spectra and the feed compositions. Again, this reflects the statistically random nature of the polymerizations and the quantitative yields obtained.

Figure S4 shows a comparison of the FTIR spectra of PBTC10, **4b**, **4d**, **4g**, and PBZT. The characteristic peaks together with their assignments are listed in Table S1. As would be expected, the copolymers have vibrational bands that are found in either PBZT or PBTC10, the intensities of which vary with composition. There are stricking differences between the spectra of

* To whom correspondence should be addressed.

† Current address: General Electric Research and Development, P.O.Box 8, Schenectady, New York 12301.

PBZT and PBTC10, for example, the bands at 1465, 1162 and 722 cm^{-1} which are due to CH_2 scissoring, twisting and rocking, respectively[22], in PBTC10 are absent in PBZT. On the other hand, the bands in PBZT which have been assigned[23] to the C=C stretch of the 1,4-phenylene ring (1484 cm^{-1}), the "crystalline" band (1250 cm^{-1}), the heteroring "breathing" (960 cm^{-1}), and the out-of-plane C-H bend of the 1,4-phenylene ring (838 and 704 cm^{-1}), are absent in PBTC10. The heteroring breathing is the strongest band in PBZT and its intensity decreases linearly as the PBZT content is reduced in the rod-coil copolymers. The intensity of this band provides a measure of the "rigidity" of the rod-coil copolymer chains since its absence in PBTC10, shows the flexible-coil limit, in which the benzobisthiazole breathing mode does not result in any change in dipole moment. The bands at 1532 and 1055 cm^{-1} in PBZT were tentatively assigned in the literature to the 1,4-phenylene ring.[23] However, comparing the FTIR spectra of PBZT with PBTC10 and the copolymers **4**, the prior assignment of these bands appears to be incorrect. The band at 1532 cm^{-1} in some thiazole compounds have been assigned to the thiazole ring vibrations.[24] The fact that this band increases in intensity as the PBZT content in the copolymers **4** is reduced, suggests that this band is due to the benzobisthiazole ring vibrations and not the 1,4-phenylene ring. The band at 1056 cm^{-1} is not as sensitive to composition and may be due to both the 1,4- and 1,2,4,5- substituted benzene rings.

Although the primary use of IR spectroscopy is for the identification of the characteristic bands of different functional groups, quantitative information can also be derived since the absorption intensities of each vibrational mode follows Beer's law.[25] In order to avoid the inherent assumption of photomeric linearity and accuracy of the spectrometer, a characteristic band that is not overlapped by any other band in the spectrum can be used to normalize the intensities.[25] We have utilized the ratio method for the quantitative determination of the composition of the copolymers by using two bands that are found in the FTIR spectra of PBZT and the copolymers **4** but not in PBTC10. We normalized the heteroring "breathing" band at 960 cm^{-1} in each copolymer with the band at ~840 cm^{-1} which is due to the out-of-plane C-H bend of the 1,4-phenylene ring. By comparing this normalized intensity to that of the pure PBZT, the rod-coil

copolymer composition, i.e. $f = x/(x+y)$, is inferred. A plot of the relative FTIR intensities versus the feed composition (not shown) gave a linear relationship, which is an independent check on the results obtained from ^{1}H NMR.

Figure S5 shows a comparison of the FTIR spectra of PBTC10, **5b**, **5d**, **5g**, and PBTPV. The characteristic peaks together with their assignments are listed in Table S2. The FTIR absorption bands in copolymers **5** are essentially a superposition of the component spectra of PBTPV and PBTC10, the intensities of the bands varying with copolymer composition. The FTIR bands due to the asymmetric stretches of the *trans*-vinylene linkage in PBTPV which appear at ~1624 cm^{-1}, is absent in PBTC10. The same is true for the bands due to the 1,4-phenylene ring (1489 cm^{-1}), the "crystalline" band (1230 cm^{-1}), the heteroring "breathing" (949 cm^{-1}) in PBTPV and the copolymers **5**. Comparing the FTIR spectra of copolymers **4** and **5**, the features which are due to the same flexible coil component, PBTC10, can be seen with slight shifts in the vibrational frequencies due to the differences in the rod-coil chain environment. The differences between the 1,4-phenylene and 1,4-phenylenebisvinylene linkages is reflected in the asymmetric C=C stretch in **5** and a slight shift of the other characteristic bands listed in Tables S1 and S2.

Figure S6 shows the region of the ^{1}H NMR spectra where the benzobisthiazole proton resonances appear (δ=8.9-9.3 ppm) in copolymers **4b**, **4d**, and **4e**. Additional insight into the molecular structure of the copolymers was obtained from ^{13}C NMR spectra. Figure S7 shows the ^{13}C NMR spectrum of homopolymer **2** (PBTC10) with the assignment of the chemical shifts.[29] The spectrum was acquired over 14 h; the noise level is due to the high viscosity of the solution, ~5 wt% polymer in deuterated nitromethane-$AlCl_3$. The number of carbon resonances is consistent with the proposed structure. Figure S8 shows the ^{13}C NMR spectrum of **4c** obtained under the same conditions as for **2**. The inset A in Figure S8 shows an expansion of the resonances due to the methylene carbons, showing similar features with that of **2**. Inset **B** in Figure S8 shows the region of the chemical shifts due to 1,4-phenylene ring in **4c** and **4e**. The differences in the chemical shifts (δ=130.95-131.16 ppm) of **4c** and **4e** is due to the increased π-conjugated sequence in **4e** compared to **4c**, in agreement with other characterizations. There was no

significant differences between the resonances due to the carbons in the benzobisthiazole ring (δ = 188.42-188.85 ppm) in **4c** and **4e**. This is apparently due to the effect of coordination of the Lewis acid ($AlCl_3$) to the heteroatoms of the benzobisthiazole rings.

Figure S9 shows the TGA thermograms of copolymers **4** and corresponding homopolymers (PBTC10 and PBZT) which were obtained in flowing nitrogen atmosphere at a heating rate of 10 °C/min. Figure S10 shows typical DSC thermograms of PBTC10, **4b**, **4c**, **4g**, and PBZT. Figure S11 shows the WAXD patterns of films of several copolymers along with the pure PBTC10. Cyrstalline peaks characteristic of either the coillike or rodlike homopolymers (**2** and **1**) could not be detected. The characteristic d-spacings of aggregated PBZT repeat units, previously reported at 5.85 and 3.54 Å (the (100) and (010) reflections),[31] were not found in the copolymers. The WAXD patterns of the copolymers exhibit broad amorphous halos in the two-theta region of 10-27°, indicative of amorphous materials down to the 0.7 nm scale. From the peak broadness, d-spacings of 4.0-4.1 Å and lateral coherence length of 0.7 nm can be estimated.

Sequence Length Distribution Model. Step copolymerization of monomer mixtures such as that involving 2,5-diamino-1,4-benzenedithiol, 1,10-decanedicarboxylic acid and terephthalic acid or 1,4-phenylene diacrylic acid, is expected to result in a *random segmented copolymer* irrespective of the differences in the reactivities of the monomers.[27] Thus, we can derive an expression for the sequence lengths from probability considerations as follows. Let p be the probability that a condensation reaction occurs between terephthalic acid or 1,4-phenylene diacrylic acid monomer (B) and (1-p) the probability that the conjugated sequence is terminated by 1,10-decanedicarboxylic acid monomer (A). A schematic illustration of the possible ways of attaching monomer B to form a conjugated dimer , assuming that the probabilities are independent and remain fixed irrespective of previous outcome, is as shown below.

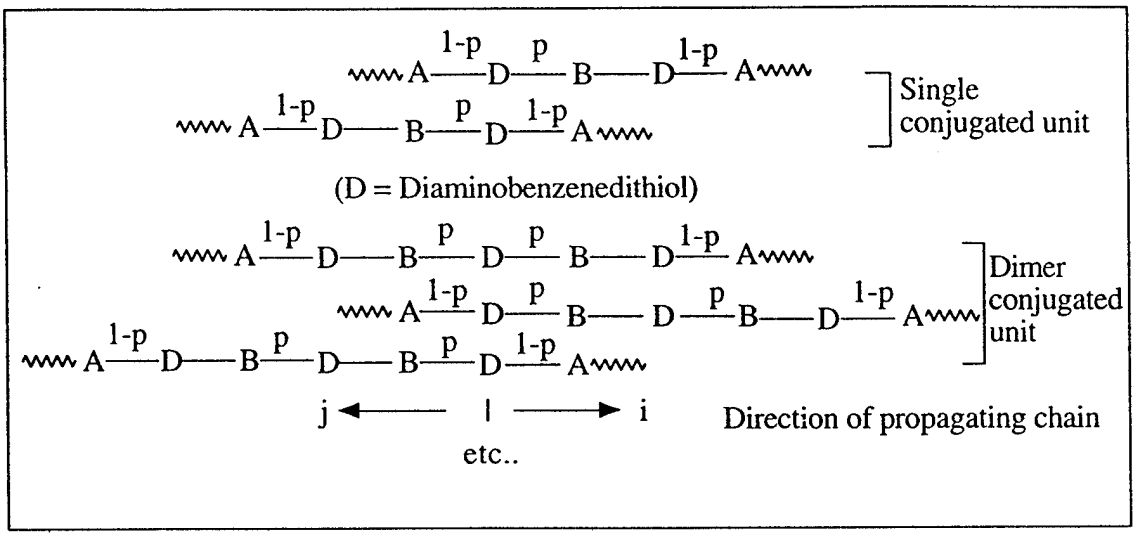

Let P(n) be the probability that a sequence incorporating n conjugated B units have been formed. Then, for a sequence with single conjugated unit (i.e. n = 1), two termination steps occur after monomer B adds on either side of D:

$$P(1) = p(1-p)^2 + p(1-p)^2$$
$$= 2p(1-p)^2 \qquad (1)$$

To form a sequence with n = 2 , monomer B can add on each side of D before two termination steps occur, or two B's can add on the same side of a propagating chain before termination occurs. Thus,

$$P(2) = p^2(1-p)^2 + p^2(1-p)^2 + p^2(1-p)^2 \qquad (2)$$
$$= 3p^2(1-p)^2$$

If we consider the propagation in two directions i and j of a chain, then the probability of finding a sequence of n conjugated units is

$$P(n) = \sum_{x_i=0}^{n} \sum_{x_j=0}^{n} [p^{x_i}(1-p)][p^{x_j}(1-p)]\delta(x_i + x_j - n) \qquad (3)$$

$$\delta(x_i + x_j - n) = 0 \text{ for } x_i + x_j \neq n$$
$$= 1 \text{ for } x_i + x_j = n$$

$$P(n) = \sum_{x_i = 0}^{n} [p^{x_i}(1-p)][p^{n - x_i}(1-p)]$$

$$= \sum_{x_i = 0}^{n} p^n(1-p)^2$$

$$P(n) = (n+1)p^n(1-p)^2 \qquad ; \sum_{x_i}^{\infty} P(n) = 1 : 0 < p < 1 \qquad (4)$$

Evaluating P(1) and P(2) from Equation (4) gives the same result as Equations (1) and (2), and in particular, P(0), which is the probability that a sequence starting with D has no B units, is equivalent to having two or more termination steps in sequence ($P(0) = (1-p)^2$). Since condensation polymerization is independent of reactivity, the probability p is the monomer feed ratio.[27]

Table S1. Summary of Characteristic FTIR bands (600-2000 cm^{-1}) of homopolymers **1** and **2** and copolymers **4**.

Assignment	**1**	**2**	Copolymers **4**	Comments
Heteroring Vibrations	1532 (w)	1533 (vs)	1532 (vs)	Decreases with increasing composition[a]
1,4-C_6H_4 C=C Str.	1484 (vs)	-	1483 (s)	Increases with composition
δ_s-CH_2 scissoring	-	1465 (m)	1465 (m)	Decreases with increasing composition
1,2,4,5-C_6H_2	1427 (m)	1427 (s)	1428 (s)	"
Heteroring str.	1400 (s)	1404 (s)	1401 (s)	-
Heteroring str.	1313 (vs)	1310 (s)	1312 (vs)	Increases with composition
"Crystalline" band	1250 (m)	-	1250 (m)	Weak up to 50% composition
CH_2 twisting	-	1162 (m)	1161 (m)	Decreases with increasing composition
1,4-C_6H_4 1,2,4,5-C_6H_2	1056 (m)	1055 (s)	1056 (m)	"
Heteroring breathing	960 (vs)	-	960 (vs) 948 (sh)	Increases with composition

1,2,4,5-C_6H_2	860 (s)	857 (s) 845 (sh)	859 (s)	"
1,4-C_6H_4	838 (s)	-	839 (s)	"
CH_2 rock	-	722 (m)	721 (w)	Decreases with increasing composition
1,4-C_6H_4	704 (m)	-	703 (m)	Increases with composition

vs = very strong; s = strong; m = medium; w = weak; sh = shoulder; Str. = stretch.

a. Composition refers to mole% **1** (PBZT).

Table S2. Summary of Characteristic FTIR bands (600-2000 cm^{-1}) of homopolymers **2** and **3** and copolymers **5**.

Assignment	**3**	**2**	Copolymers **5**	Comments
Asymm. *trans*-vinylene str.	1623 (vs)	-	1624 (s)	Increases with composition[a]
Heteroring Vibrations	1516 (s)	1533 (vs)	1528 (vs) 15316 (m)	Shifts towards **2** with decreasing composition
1,4-C_6H_4 C=C Str.	1489 (vs)	-	1490 (s)	Increases with composition
δ_s-CH_2 scissoring	-	1465 (m)	1465 (m)	Decreases with increasing composition
1,2,4,5-C_6H_2	1418 (m)	1427 (s)	1426 (s)	"
Heteroring str.	1403 (s)	1404 (s)	1404 (s)	-
Heteroring str.	1312 (vs)	1310 (s)	1310 (vs)	Increases with composition
"Crystalline" band	1231 (m)	-	1230 (m)	Weak up to 50% composition
CH_2 twisting	-	1162 (m)	1161 (m)	Decreases with increasing composition
1,4-C_6H_4 1,2,4,5-C_6H_2	1056 (m)	1055 (s)	1056 (m)	"

Heteroring breathing	949 (vs)	-	950 (vs)	Increases with composition
1,2,4,5-C_6H_2	855 (s)	857 (s) 845 (sh)	858 (s)	"
1,4-C_6H_4	827 (s) 804 (m)	-	827 (s) 805	"
CH_2 rock	-	722 (m)	721 (w)	Decreases with increasing composition

vs = very strong; s = strong; m = medium; w = weak; sh = shoulder; Str. = stretch.

a. Composition refers to mole% **3** (PBTPV).

Figure Captions

Figure S1. ^{1}H NMR spectrum of copolymer **4f** in $CD_3NO_2/AlCl_3$ and its assignments.

Figure S2. ^{1}H NMR Spectrum of copolymer **5f** in $CD_3NO_2/AlCl_3$ and its assignments.

Figure S3. ^{1}H NMR integration versus Feed composition of copolymers **5a-5h**.

Figure S4. FTIR absorption spectra of PBTC10, **4b**, **4d**, **4g**, and PBZT.

Figure S5. FTIR absorption spectra of PBTC10, **5d**, **5f**, and PBTPV.

Figure S6. ^{1}H NMR spectra of copolymer **4b**, **4d**, and **4e** in $CD_3NO_2/AlCl_3$ showing resonances between 8-10 ppm: (a) 4b; (b) 4d; (c) 4e.

Figure S7. ^{13}C NMR spectrum of PBTC10 in $CD_3NO_2/AlCl_3$ and its assignments.

Figure S8. ^{13}C NMR spectrum of **4c** in $CD_3NO_2/AlCl_3$ and its assignments. Inset A: region of the central methylene carbons; Inset B: region of the 1,4-phenylene ring for **4c** and **4e**.

Figure S9. TGA thermograms of (1) PBZT, (2) **4h**, (3) **4e**, (4) **4c**, (5) PBTC10 heated in nitrogen atmosphere at 10 °C/min.

Figure S10. DSC Thermograms of (1), PBTC10; (2), **4b**; (3), **4c**; (4), **4g**; (5), PBZT.

Figure S11. Wide angle X-diffraction patterns of several copolymers **4** and PBTC10. (1), PBTC10; (2), **4b**; (3), **4c**; (4), **4d**; (5), **4g**.

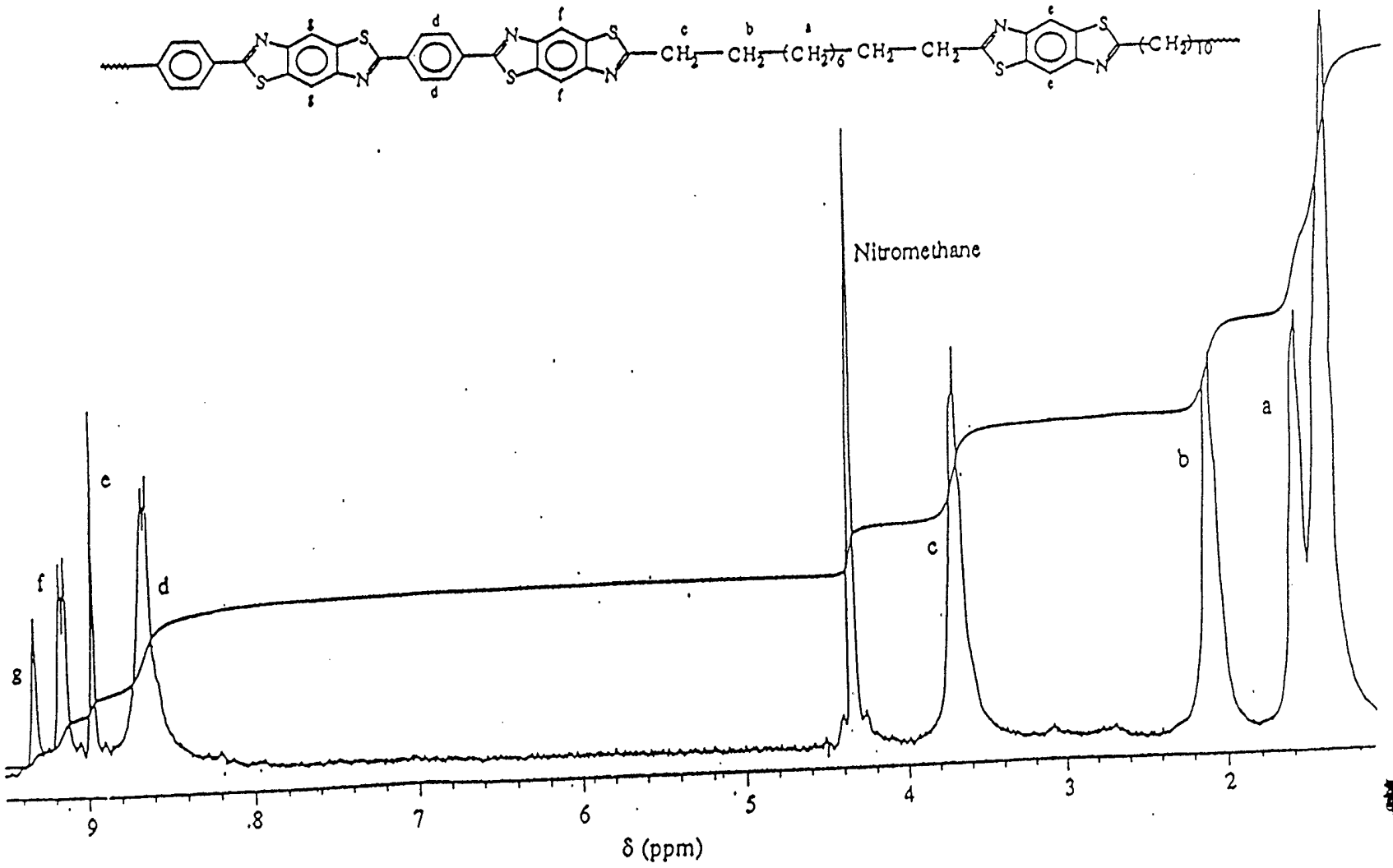

Figure 2. ^1H NMR spectrum of copolymer **4f** in $CD_3NO_2/AlCl_3$ and its assignments.

Fig. 2

(S1)

Fig. 4 (S2)

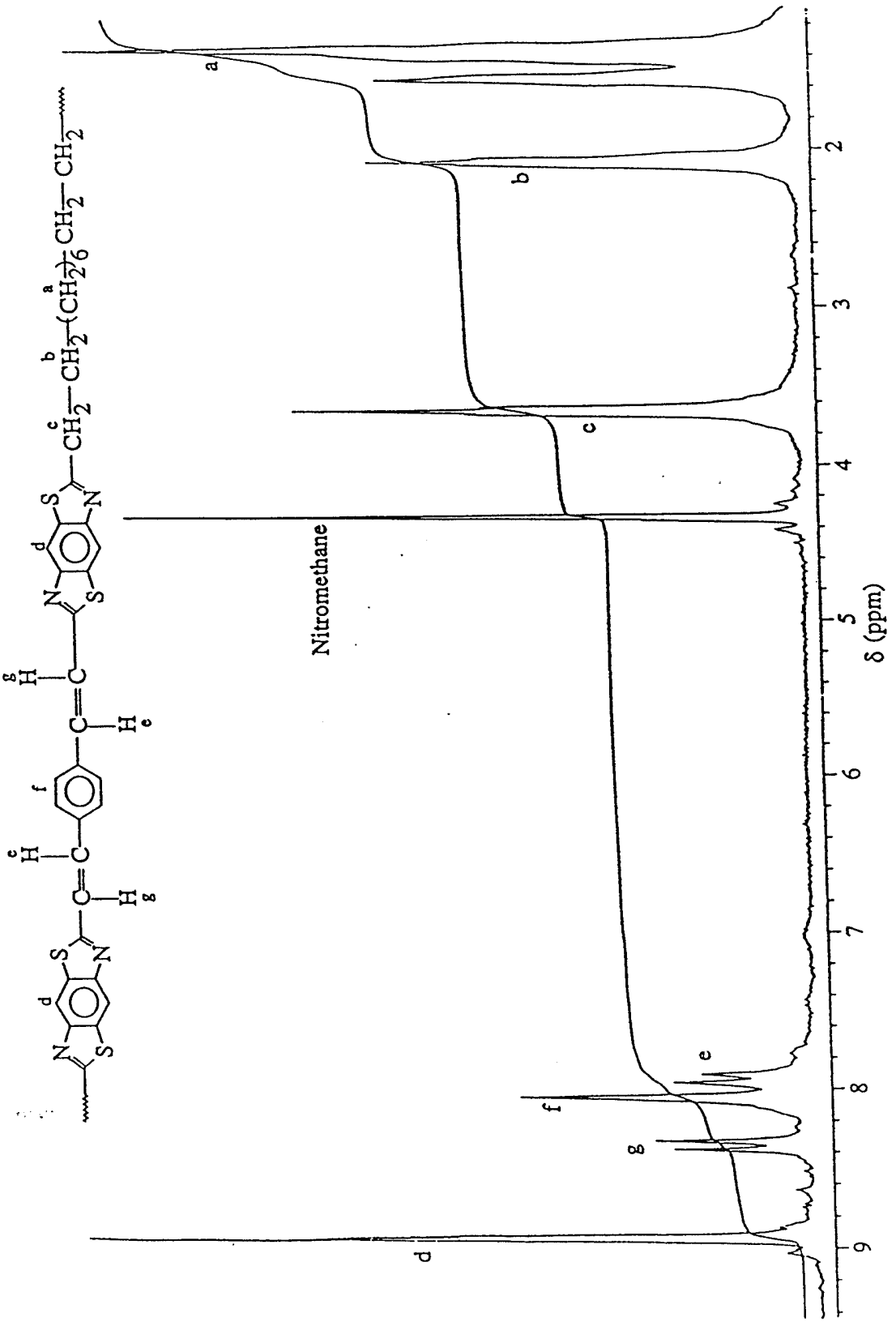

Fig. 5 (S3)

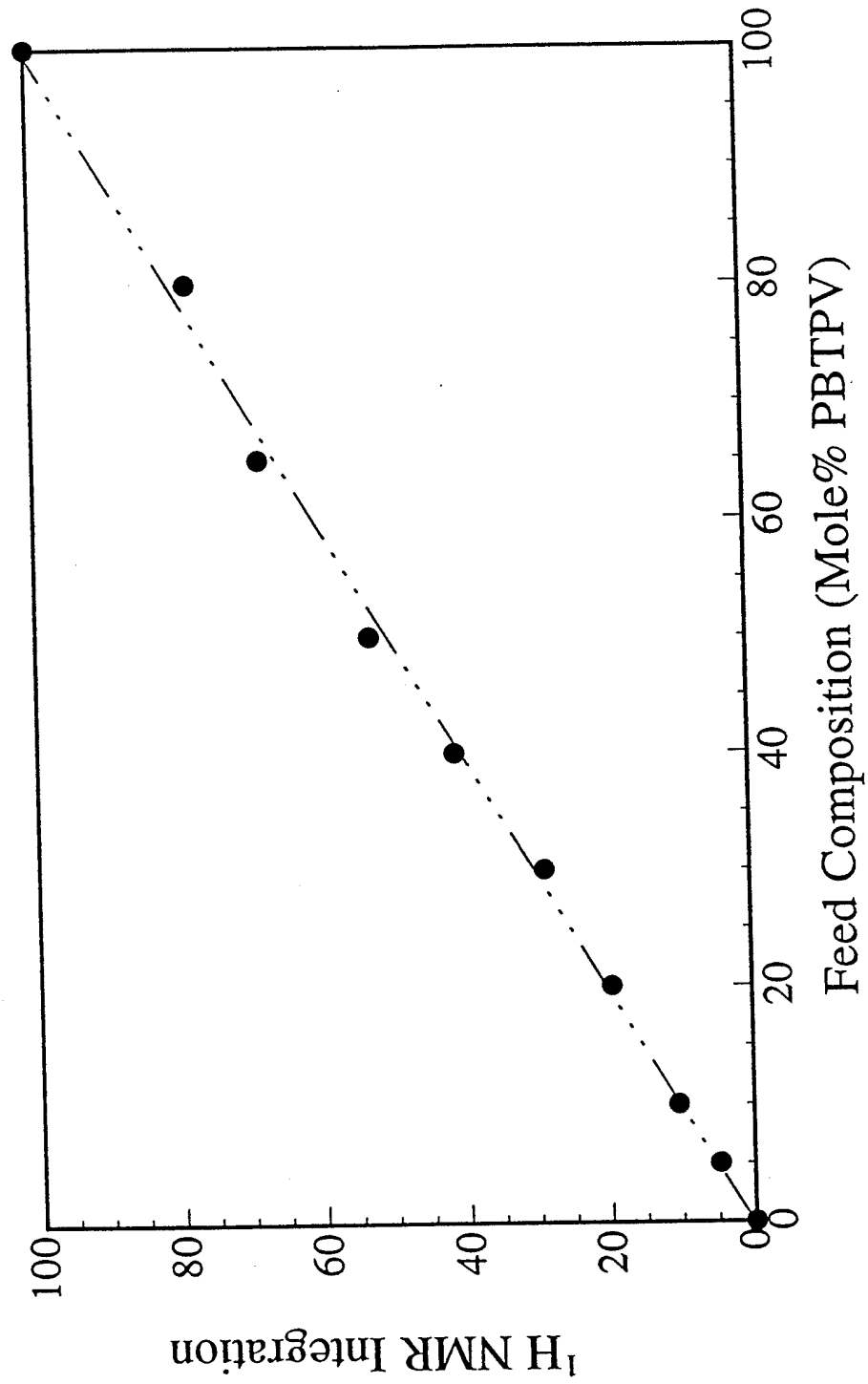
^{1}H NMR Integration
0
20
40
60
80
100
Feed Composition (Mole% PBTPV)
0
20
40
60
80
100

Fig. 6
(S4)

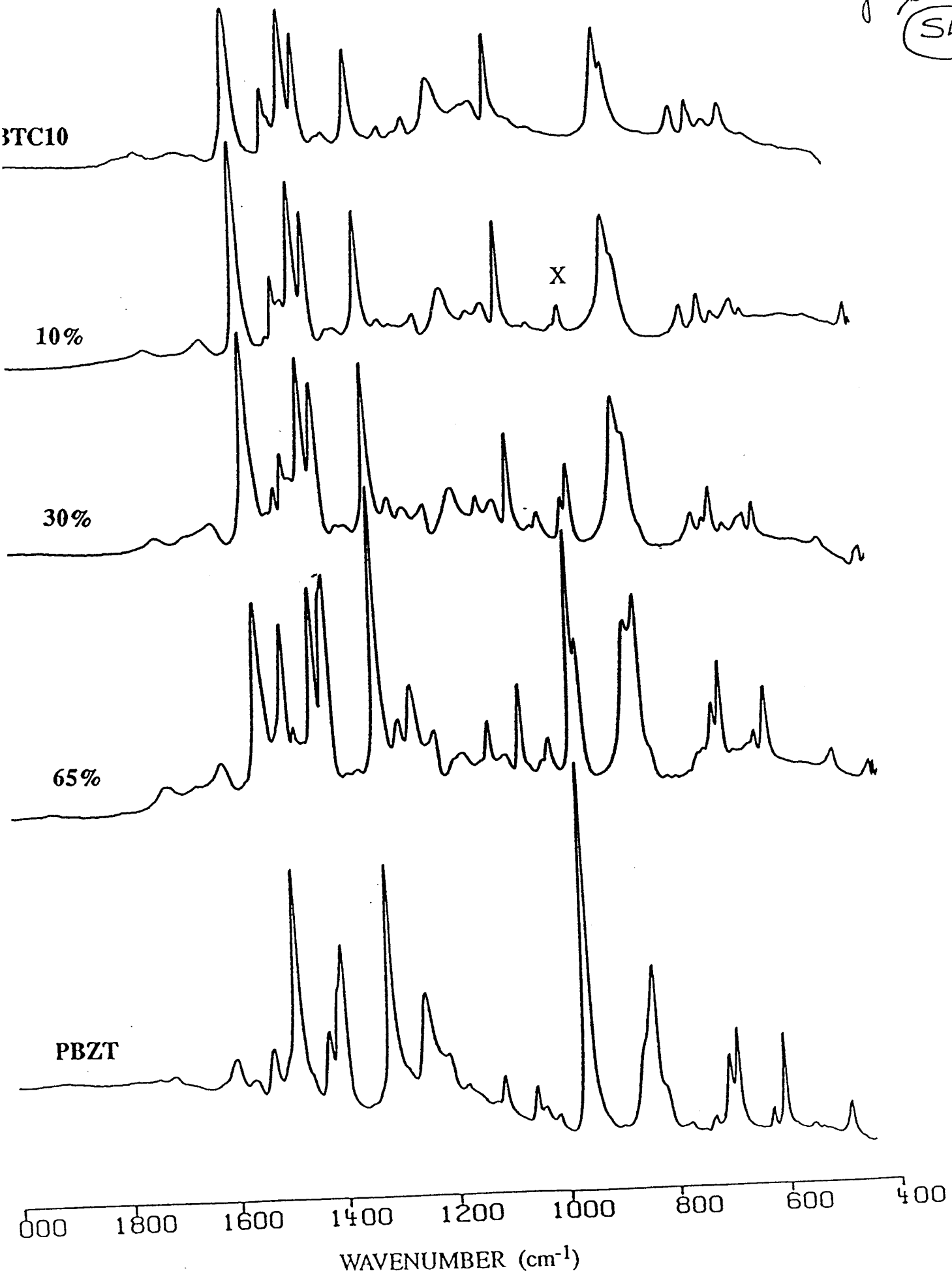
3TC10
10%
30%
65%
PBZT
X
000
1800
1600
1400
1200
1000
800
600
400
WAVENUMBER (cm-1)

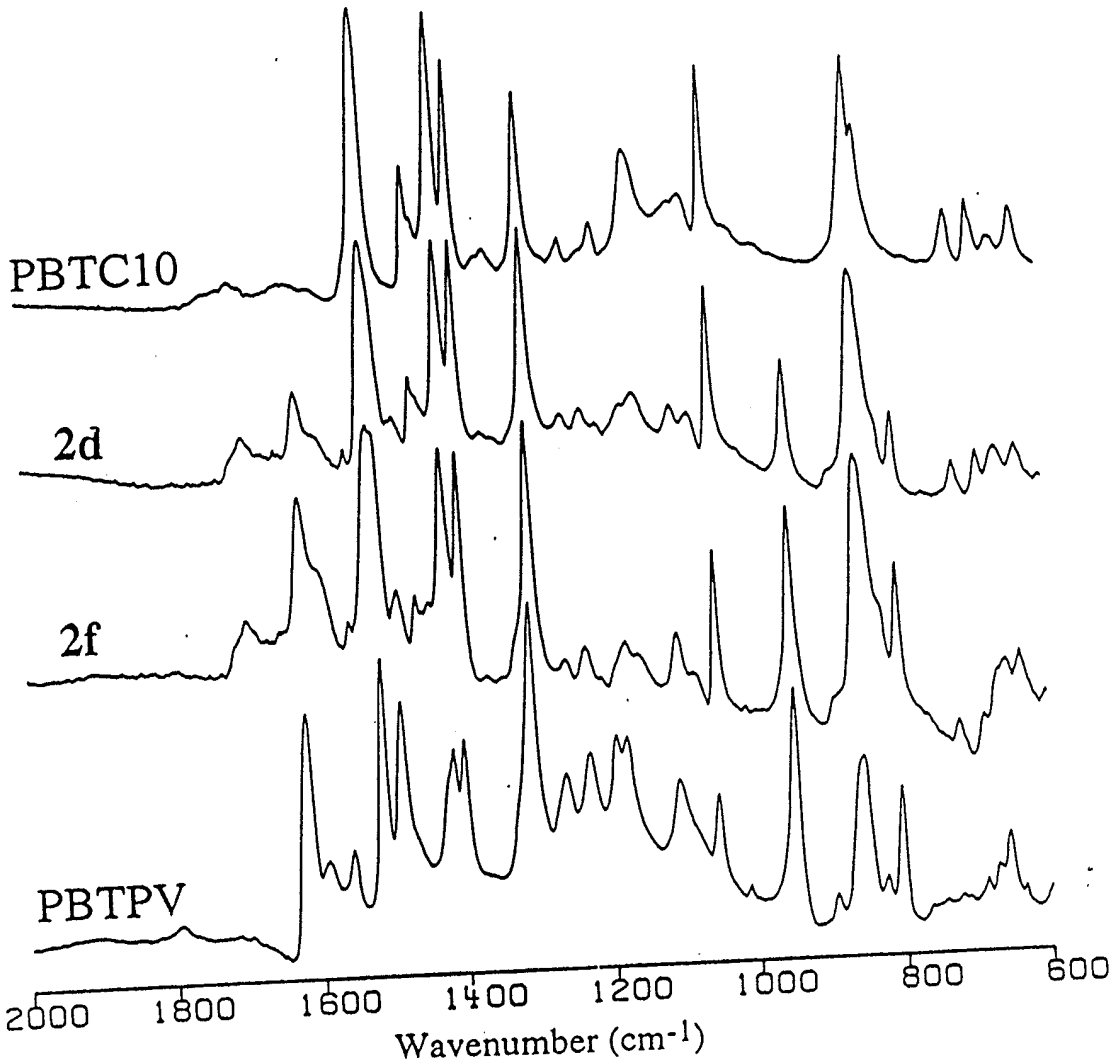

Figure 7. FTIR absorption spectra of PBTC10, **5d**, **5f**, and PBTPV.

Fig. 7

S5

Fig. ~~10~~ 56

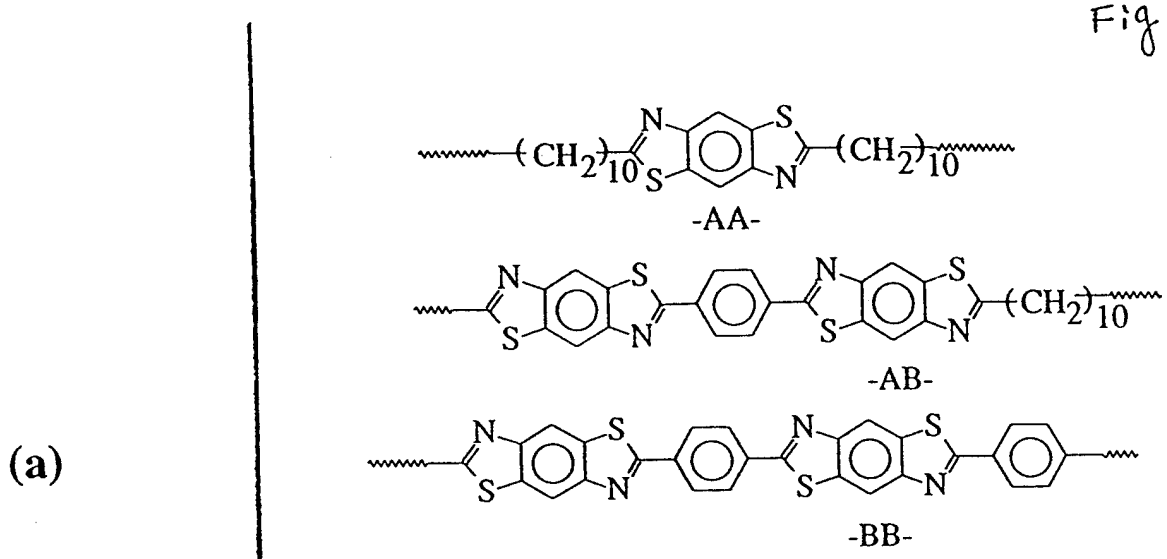

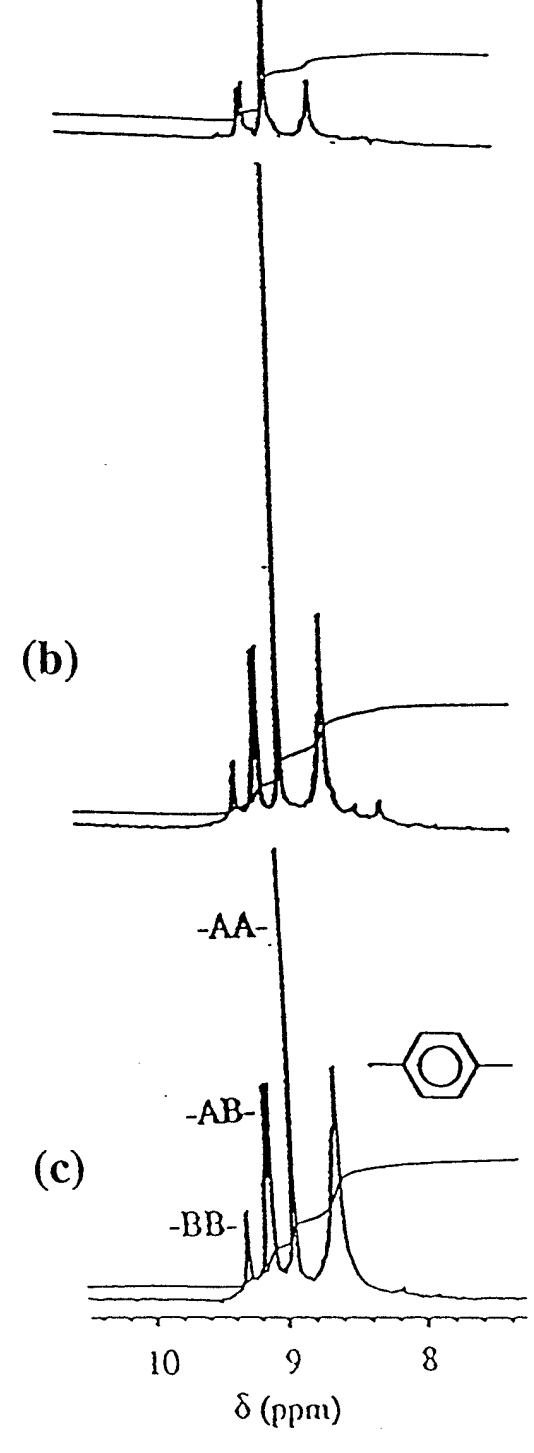

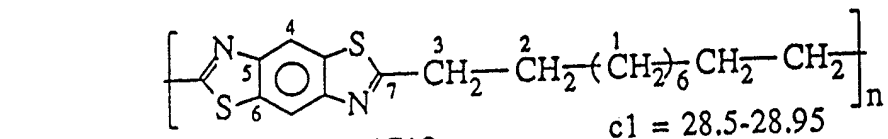

PBTC10

c1 = 28.5-28.95
c2 = 29.01
c3 = 32.11
c4 = 113.41
c5 = 131.8
c6 = 138.17
c7 = 188.35

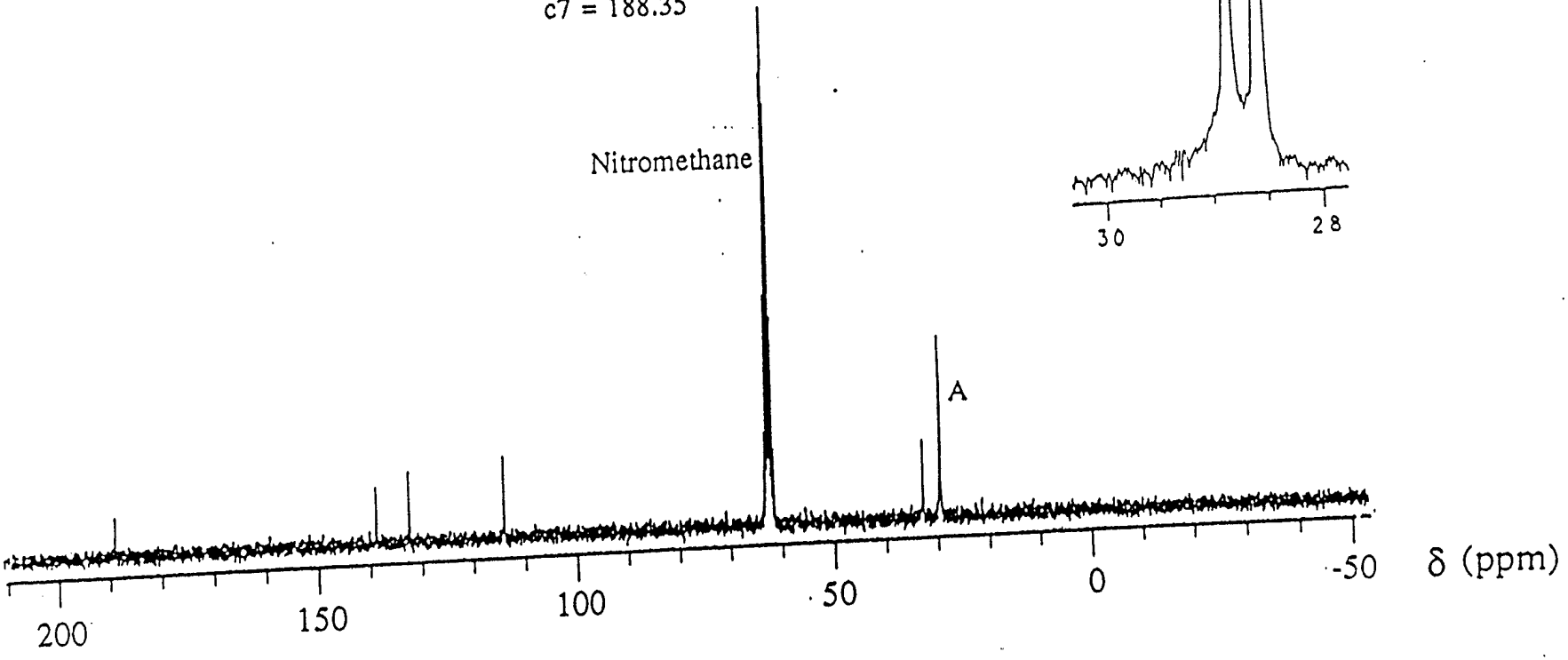

Fig. 15

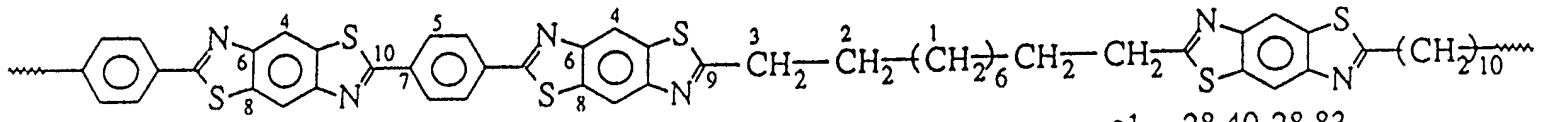

c1 = 28.40-28.83
c2 = 29.01-29.04
c3 = 32.11-32.23
c4 = 113.41-113.42
c5 = 130.95-131.16
c6 = 131.78
c7 = 132.78
c8 = 138.17
c9 = 188.3
c10 = 188.42-188.85

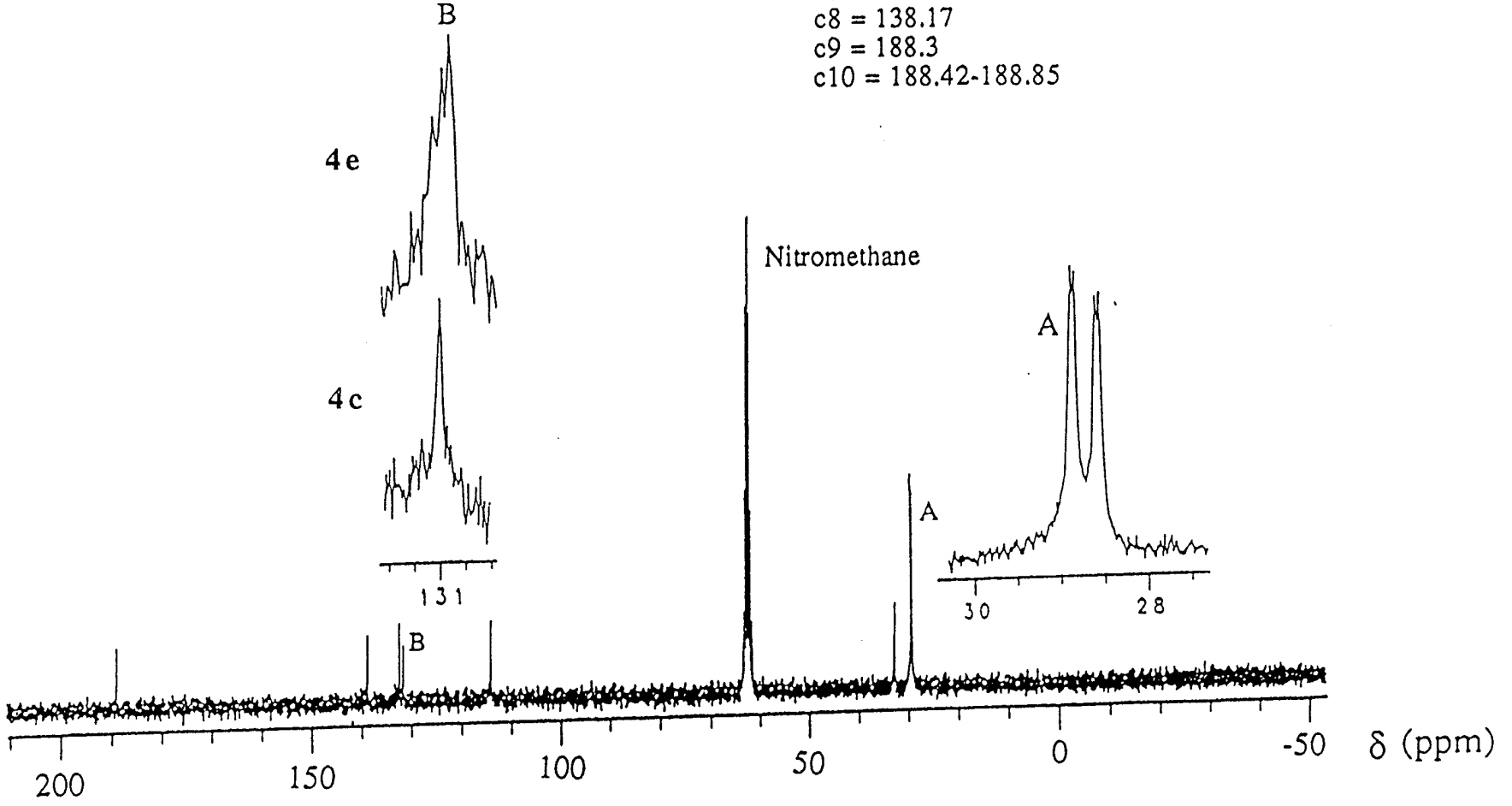

Fig. 8

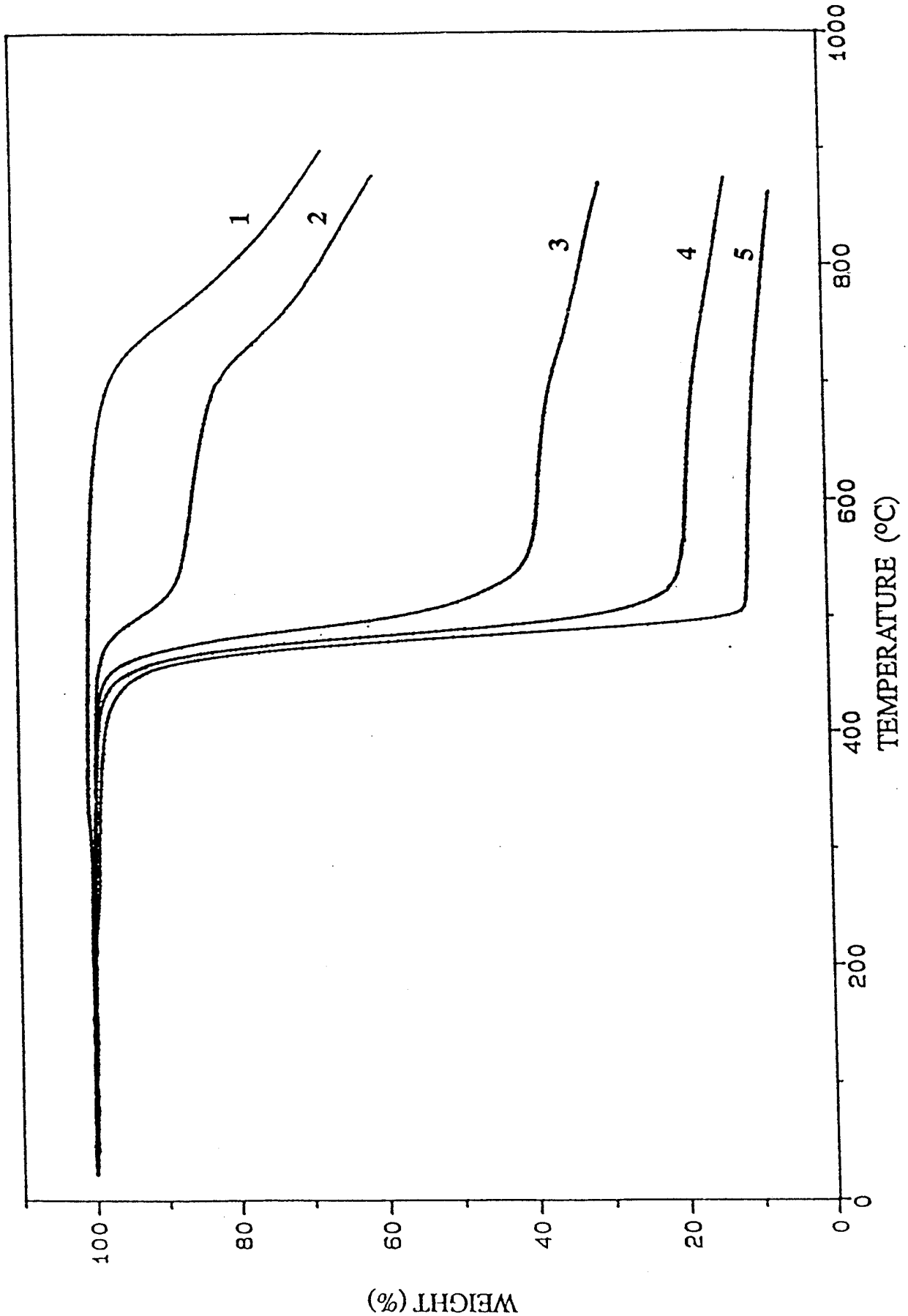
WEIGHT (%)
100
80
60
40
20
0
0
200
400
600
800
1000
TEMPERATURE (°C)
1
2
3
4
5

Fig. ~~15~~ 10

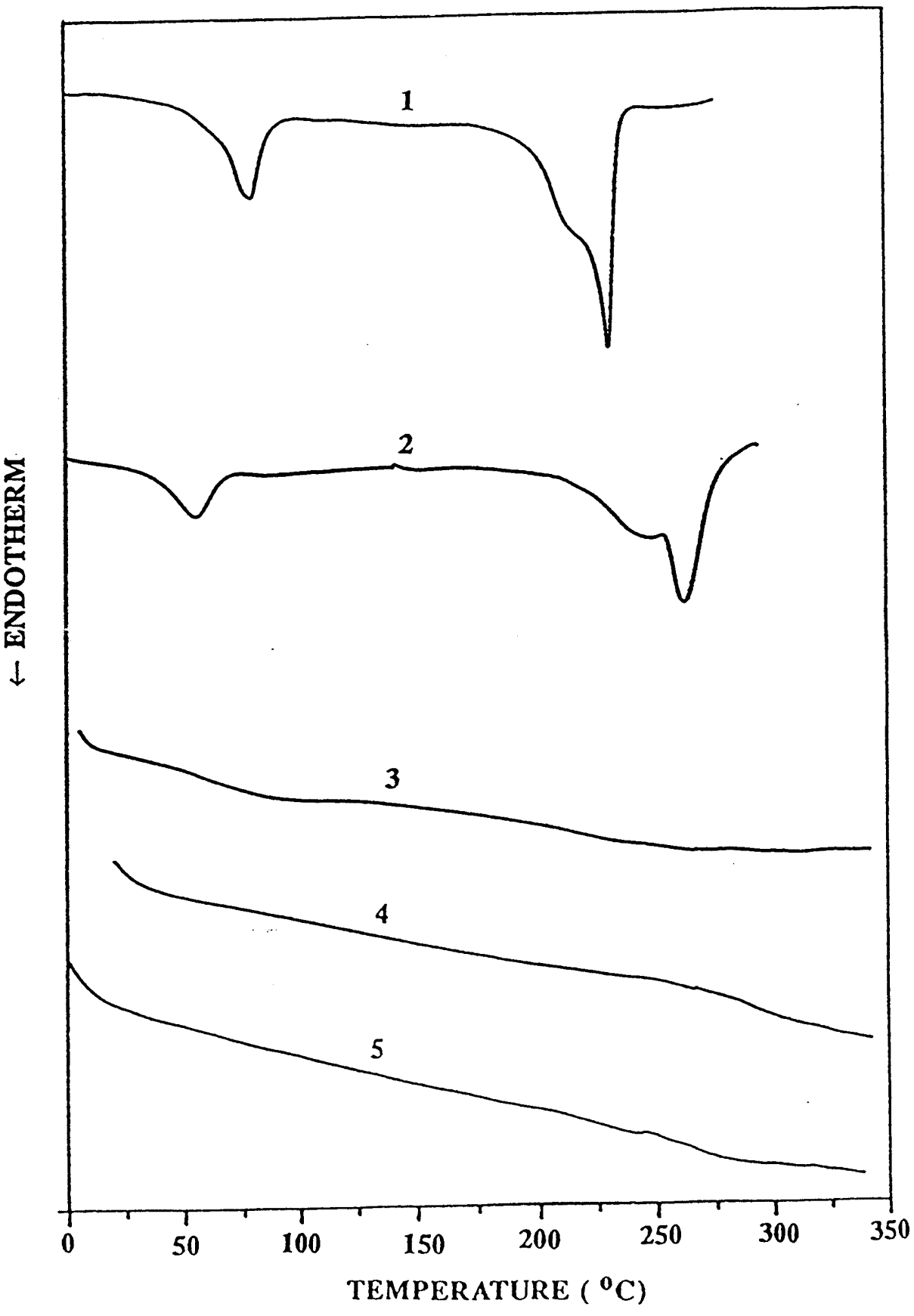

Fig (S11)

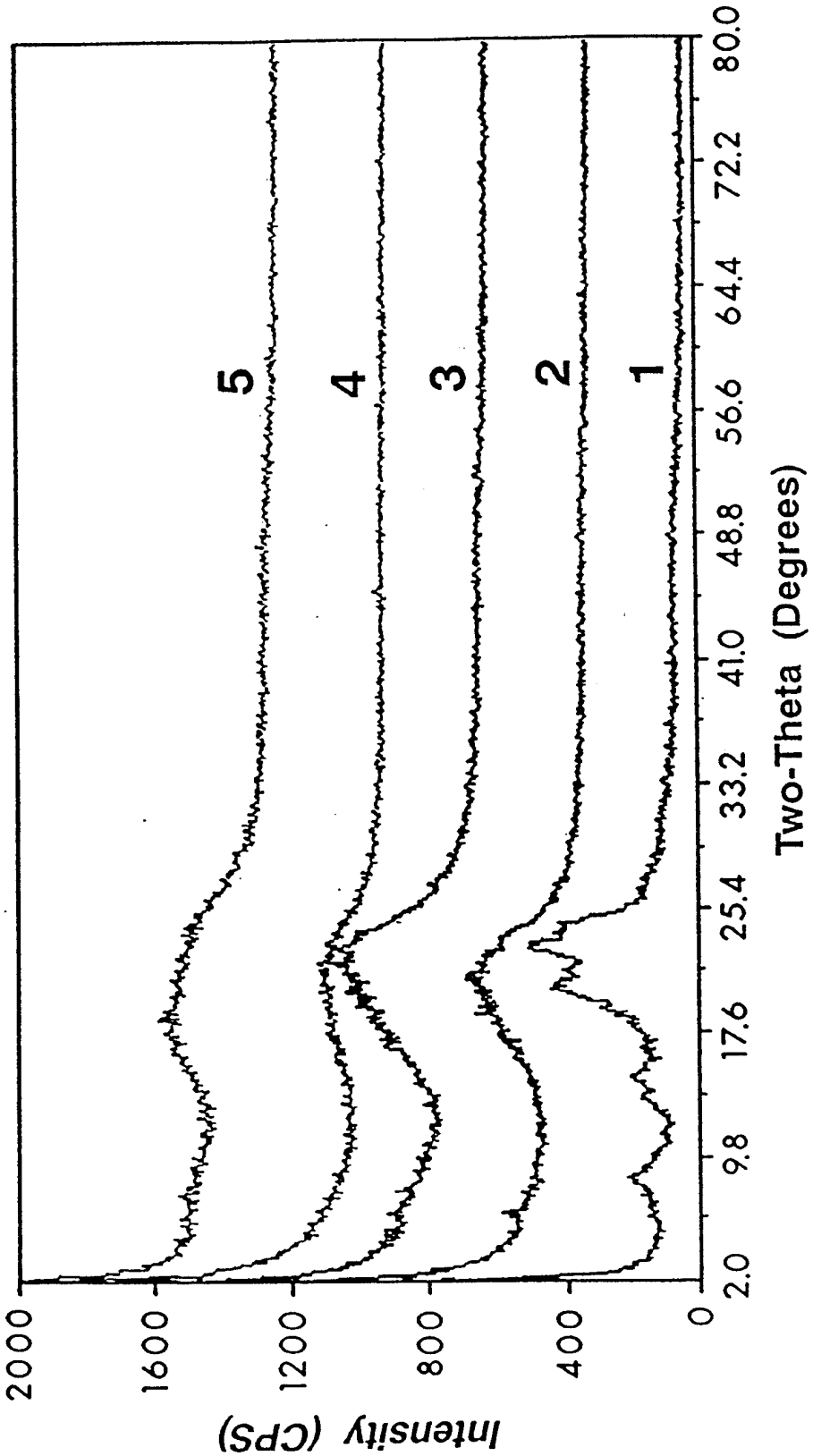

Figure #6 (S11)

Jeneklve & Osaheni